IONIC MODEL FOR CHROMIUM, MANGANESE AND IRON IMPURITIES IN COPPER

BY

DANIEL CORNELIUS ABBAS

A.B., Calvin College, 1969
M.S., University of Illinois, 1970

THESIS

Submitted in partial fulfillment of the requirements
for the degree of Doctor of Philosophy in Physics
in the Graduate College of the
University of Illinois at Urbana-Champaign, 1977

Urbana, Illinois

DISCLAIMER

IONIC MODEL FOR CHROMIUM, MANGANESE AND IRON IMPURITIES IN COPPER

Daniel Cornelius Abbas, Ph.D.
Department of Physics
University of Illinois at Urbana-Champaign, 1977

We have discovered that the NMR frequencies of Cu atoms which are near neighbors to Cr atoms in dilute CuCr have an anomolous temperature dependence. Comparison with data from CuMn and CuFe which display the normal temperature dependence of a Curie-Weiss law lead us to conclude that an ionic model of the magnetic impurity is necessary to explain the data. We develop a model which assumes a definite $3d^n$ configuration with a definite L-S ground state and includes intraconfigurational energy level splittings due to a crystalline electric field and spin-orbit coupling. We calculate the spin and orbital susceptibilities from the ionic structure and include the effects of the impurity electron-conduction electron mixing interaction in a perturbation treatment. We also calculate the impurity hyperfine fields expected from the model. Comparison of the model predictions with the data lead us to conclude that (a) Cr and Mn have the structure which corresponds to the free ion divalent configuration while Fe corresponds to a monovalent configuration, (b) the crystal field at the site of the magnetic atoms is opposite of that usually assumed, and (c) the Weiss temperature of CuCr is 2.9 ±1.0 K which is higher than most previously reported values but agrees within the experimental errors with a recently published bulk magnetic susceptibility measurement.

ACKNOWLEDGMENTS

I gratefully acknowledge the guidance and assistance of Professor C. P. Slichter who directed this thesis. His seemingly boundless enthusiasm for physics is contagious and helps to rekindle drive at times when research becomes bogged down in onerous experimental problems such as equipment failure. His ability to reduce complex physical phenomena to a simple illustrative example and his demand that his students do likewise has given me a deeper insight into physics and a greater appreciation of its fascination.

I also thank the other members of the Slichter group whom it has been my pleasure to know for many stimulating discussions. I especially acknowledge Dr. David Follstaedt who first taught me the basics of NMR and Dr. Thomas Aton whose earlier experiments motivated this thesis.

I thank Professsors Roger Griffioen and Vernon Ehlers for first stimulating my interest in physics and for giving me a basic foundation on which to build.

I thank my parents for their concern that I get a good education and the sacrifices they made to make it possible. Finally, I thank my wife, Betti, for her encouragement during difficult times and especially for bearing more than her share of the responsibilities to the family during the past few years.

This work was supported by the U. S. Energy Research and Development Administration under Contract E(11-1)-1198.

TABLE OF CONTENTS

Page

1. INTRODUCTION

Iron group atoms in insulators are now well understood. The same is not true when the host is a metal. The experimental methods which have been so important for insulating hosts do not reveal enough information (ESR) or do not work (ENDOR) in metallic hosts. We have studied the NMR of Cu atoms which are near neighbors to Cr atoms in dilute alloys of Cr in Cu. Our discovery that the NMR frequencies of these atoms have an anomolous temperature dependence compared with those found for Cu atoms which are near neighbors to Mn or Fe atoms in similar dilute alloys led us to a theoretical analysis from which we are able to deduce for the first time a detailed picture of the electronic structure of these and other iron group atoms in Cu.

The understanding of dilute alloys of magnetic impurities in nonmagnetic metal hosts is far from complete. The term "magnetic" itself needs further clarification when applied to a magnetic impurity which is placed in a nonmagnetic metal. The mixing interaction between the impurity electrons and conduction electrons tends to reduce the magnetic nature of the impurity atom, and if the mixing is strong enough, an impurity which is magnetic when placed in an insulating host becomes nonmagnetic in the metal host. The mixing interaction also produces an antiferromagnetic polarization of the conduction electrons with the result that the impurity magnetic susceptibility which obeys a Curie law in an insulator host obeys a Curie-Weiss law in the metal. Although the possibility of high Weiss temperatures which can make the alloy appear nonmagnetic over the temperature range which is experimentally accessible makes determination of the magnetic or nonmagnetic nature of some alloys difficult, we leave the nature of the alloys which show only slight temperature variation to their susceptibilities unspecified and adopt

the empirical definition that those alloys which exhibit a definite Curie-Weiss law are magnetic. In particular, we consider CuCr, CuMn and CuFe which have Weiss temperatures of approximately 3 K, 10 mK and 28 K respectively to be magnetic.

The absence of detailed experimental knowledge of the magnetic atoms in nonmagnetic metals has permitted a variety of theoretical descriptions, differing principally in the nature of the assumptions about the magnetic atom and its interaction with the electrons of the host metal conduction band. Historically three models have been of particular importance: (1) the so-called "s-d" model, (2) the Friedel-Anderson model, and (3) the Hirst model. All three models may be described in terms of the general Hamiltonian:

$$H = H_{el} + H_{imp} + H_{mix} \quad , \tag{1.1}$$

where H_{el} describes the conduction electrons, H_{imp} describes the impurity, and H_{mix} describes the mixing between the conduction electrons and the impurity electrons. For the iron group impurities, to which we are restricting this discussion, the important mixing is that between the impurity d electrons and components of the conduction electron wave functions which may be expressed as d components. H_{el} represents the kinetic energy of the conduction electrons; since it is the same for all three models, we do not discuss it in further detail at present.

The earliest attempts[1] to treat the magnetic impurity problem used the s-d model which assumes that the impurity has a net spin $\vec{S}$ and magnetic moment $g\mu_B\vec{S}$, where μ_B is the Bohr magneton and g is a constant of proportionality called the "g-value." This model makes no attempt to deduce the spin and g-value from first principles. The magnetic susceptibility of such

an atom would obey Curie's law were it not for the mixing with the conduction electrons. The form of mixing interaction assumed is an exchange interaction:

$$H_{mix} = -J \vec{S} \cdot \vec{s} \quad , \tag{1.2}$$

where J is an exchange parameter and $\vec{s}$ is the conduction electron spin. Using this form for the mixing interaction, Kondo[2] used a perturbation treatment to account for the famous minimum in the electrical resistivity which had been observed in these alloys and for the fact that the susceptibility had been found to obey a Curie-Weiss law rather than a Curie law; however at low temperatures the perturbation treatment is inadequate because it diverges and the problem becomes a genuine many-body problem. Numerous theorists struggled to find a solution to this problem, the famous "Kondo effect." Recently Krishna-murthy et al.[3] succeeded in solving the s-d model at low temperatures with a renormalization group theory approach.

Friedel[4] took the viewpoint opposite of that assumed by Eq. 1.2. He argued that the conduction bandwidth of free electrons in a metal is so large that the impurity state must fall within the band and not be localized. He treated the conduction and impurity d electrons as indistinguishable and treated the impurity problem by considering the scattering of the d electrons by the impurity potential. Scattering resonances of the potential produce virtual bound states near the impurity site. In a virtual bound state picture the question of whether or not the impurity is magnetic depends on whether or not the scattering is spin-dependent--if the scattering is spin-dependent and produces different bound states for opposite spin states, the impurity is magnetic. Friedel's approach gave no mechanism for producing such spin-dependent scattering.

Anderson[5] proposed a modification of the Friedel approach which gave such a mechanism. In its simplest form the impurity orbital state is assumed non-degenerate and one approximates

$$H_{imp} = E(n_\uparrow + n_\downarrow) + U(n_\uparrow n_\downarrow) \quad , \tag{1.3}$$

where the number operators refer to the d electrons on the impurity. The term proportional to E represents the binding energy of the Coulomb potential. The term proportional to U represents the Coulomb repulsion between opposite spin states due to the symmetric spatial part of their total two-electron wave function. Anderson uses a mixing term of the form

$$H_{mix} = \sum_{k,\sigma} V_{dk}(C^\dagger_{k\sigma} C_{d\sigma} + C^\dagger_{d\sigma} C_{k\sigma}) \quad , \tag{1.4}$$

where the $C^\dagger_{k\sigma}$ operator creates a conduction electron with wave vector k and spin σ and $C^\dagger_{d\sigma}$ creates an impurity d electron with spin σ. The coulomb term in H_{imp} tends to make the impurity magnetic while the mixing term tends to break down the magnetic moment. The relative size of these two interactions determines whether or not a moment exists. The form of the mixing (Eq. 1.4) makes the Hamiltonian a many-body Hamiltonian; Anderson treated it in Hartree-Fock approximation. With the H-F approximation, the Anderson model produces virtual bound states with a width, Δ, which is determined by the strength of the mixing interaction. The condition for the survival of a magnetic moment in the presence of the mixing interaction is then expressed in terms of the ratio U/Δ--if the ratio is large enough the moment survives. Blandin[6] expanded on Anderson's suggestions to treat the orbitally degenerate case. Coqblin and Blandin[7] have treated the orbitally degenerate Anderson Hamiltonian with a spin-orbit interaction added. Schrieffer and Wolf[8]

showed that in the strongly magnetic limit the s-d form for the mixing interaction can be derived from the Anderson form.

Anderson's model treats the Coulomb interaction as large and important. The fact that some 3d alloys do have a Curie-Weiss magnetic susceptibility and hence a magnetic moment indicates that, in terms of his model, U/Δ must be greater than unity for at least the magnetic alloys. Thus Anderson recognizes that H_{imp} is larger than H_{mix} for the magnetic alloys. Hirst[9,10] argues that if H_{imp} is larger than H_{mix} it should be treated in more detail than Anderson treats it before the mixing interaction is considered.

Hirst models the magnetic impurity atom in a metal host in close analogy to its circumstances in an insulator. In an insulator the number of d electrons on the magnetic atom is integral, depending solely on the ionic state of the atom. The magnetic atom d electron spins are coupled together to form a total spin $\vec{S}$ and the orbital angular momenta are coupled together to form a total angular momentum $\vec{L}$. The magnetic atom has a rich atomic level structure including L-S, crystalline electric field, and spin-orbit splittings. Hirst argues that the atomic structure of the magnetic atom is not that different when it is in a metallic host--the level splittings change somewhat, but the basic structure remains. The integral $3d^n$ electronic configurations will have different energies in general; designating the configuration with the lowest energy ground state as $3d^n$, the $3d^{n-1}$ and $3d^{n+1}$ configuration ground states have higher energies. The impurity electron-conduction electron interaction mixes the configurations to some extent, giving the $3d^{n-1}$ and $3d^{n+1}$ configurations a lifetime broadened level width, but the ground state cannot decay in an energy conserving process and has a narrow width produced only by virtual decay processes. If the ground state level

width is less than the splitting between the ground state $3d^n$ configuration and the first excited alternate configuration ground state, the impurity is characterized to a great extent by the $3d^n$ configuration; further if the width is less than the intraconfigurational fine structure splittings, the details of the atomic structure manifest themselves and are not obscured, contrary to widely assumed treatments with the other models. Having first treated the impurity Hamiltonian in detail, Hirst treats the mixing interaction as a perturbation.

Hirst argues that although the Anderson model is adequate for treating experimental data which are only concerned with adding or removing electrons from the impurity, it is not appropriate for treating data which are affected by the intraconfigurational details. In his review article on magnetic impurities Heeger[11] writes:

> The Anderson Hamiltonian omits spin-orbit and orbit-orbit interactions. These interactions are known to give rise to much of the details in the atomic energy level structure. However, it is doubtful that such effects are of major importance to the moment formation. Moreover, as we shall see, the experimental results do not yet call for inclusion of these interactions. In the end, however, one neglects them for the sake of simplicity and hopes for the best.

Since Heeger's article was published, careful bulk measurements have revealed that in addition to a Curie-Weiss contribution there are also temperature independent contributions to the magnetic susceptibility in CuCr[12,13] and CuFe.[14] We are unable to account for that data or our NMR data on CuCr without including the details of the atomic structure.

Just as the many-body nature of the mixing interaction has hindered understanding of the theoretical aspects of the dilute alloys, the difficulty of measurements has hindered the establishment of the experimental facts. Most of the dilute alloys are a problem metallurgically, i.e., few of the

impurities make nice, random solutions with any appreciable concentration of the impurity. The impurity atoms have a strong tendency to form clusters. Clusters of impurities often have a Curie-Weiss susceptibility with a much lower Weiss temperature than isolated impurities, and hence at low temperatures the clusters dominate the bulk susceptibility. It is only with very dilute concentrations (as low as 5 ppm) of impurities and a careful study of the concentration dependence that one can be certain one is measuring the susceptibility of isolated impurities. Bulk techniques in general are at a disadvantage for application to non-random solutions because they only measure average properties. Quantitative determinations are difficult. The Slichter group has developed satellite NMR as a technique for probing dilute alloys. It avoids the problems of bulk measurements.

By using the NMR of host nuclei which are near neighbors to isolated impurities, the Slichter group has obtained extensive experimental information about the electronic distribution around the impurities. Studies have been done on all of the iron group impurities in a copper host.[15-24] The NMR frequency of a Cu nucleus which is near a magnetic impurity atom is shifted relative to that of pure Cu by a change in Knight shift. The shift, ΔK, from the pure Cu Knight shift value, K, produces weak resonances called "satellites" in the tails of the "main line" resonance produced by Cu nuclei more distant from all impurities. In samples of metal powder ΔK arises primarily from the isotropic hyperfine coupling and hence is due to the Fermi contact interaction. It thus represents a spin polarization of the conduction electrons. Studies[18,21] have allowed the identification of the crystallographic shells which produce many of the observed satellite resonances in CuFe. Boyce and Slichter[19,20] were able to determine the temperature dependence of the impurity susceptibility and to resolve a controversy about the nature of the low temperature state

of magnetic impurities in nonmagnetic hosts--the spatial form of the conduction electron polarization is not different in the low temperature state from that at high temperatures.

During his study of CuCr near room temperature, Aton[18] found that the satellite resonances have an anomolous temperature dependence. We have followed the temperature variation of ΔK from 8.0 K to 334 K for two neighbor shells and from 8.0 K to 278 K for a third shell. For CuFe[19,20] and CuMn[18] $\Delta K/K$ obeys a Curie-Weiss law. The data from CuCr have a marked deviation from a Curie-Weiss law; however, all three satellites exhibit the same temperature dependence. We explain the observed temperature dependence in terms of an ionic model of the impurity. The basic concepts of the model are due to Hirst; however we find it necessary to modify some aspects in order to account for the behavior of CuCr, CuMn and CuFe. We demonstrate satisfactory agreement between our model and the data for all three of these alloys.

In Chapter 2 we develop the ionic model following Hirst. We discuss the treatment of the mixing interaction and the spin polarization which it produces in the conduction electrons. We describe the calculation of the spin and orbital magnetic susceptibilities, including the effects of the mixing interaction. Finally, we describe the calculation of the impurity hyperfine fields from the model.

In Chapter 3 we discuss the experimental procedures used in gathering the NMR satellite data on CuCr.

In Chapter 4 we compare the experimental data with the model developed in Chapter 2. We show that the CuCr NMR satellite data can be fit by the model and determine the model parameter values. It is necessary to choose the sign of the crystal field opposite of that assumed by Hirst. Comparison of the

bulk impurity magnetic susceptibility of CuCr, calculated from the model with no additional free parameters, with the published data shows agreement within the experimental uncertainties. Extending the model comparison to CuMn and CuFe, we find good agreement with the available data. It is also necessary to reverse the sign of the crystal field usually assumed for CuFe. Hirst assigns the ground state configuration which corresponds to a divalent ion to all of the iron group impurities. We find that Cr and Mn are indeed divalent; however we find that Fe is more likely monovalent. With this configurational assignment for Fe, the susceptibility calculated from the model agrees with the published data, and the hyperfine fields calculated from the model are in better agreement with the data then those previously calculated from other models.

Chapter 5 is a summary and a discussion of possible future experimental and theoretical work which should yield further understanding of the dilute magnetic alloys.

2. THEORY

In order to understand how information about the magnetic impurity state can be deduced from NMR satellite data, it is necessary to understand (1) the interactions which are included in the unperturbed impurity Hamiltonian, H_{imp}, (2) the effect of the mixing interaction, H_{mix}, (3) the relationship between the impurity magnetic susceptibility and the satellite data, and (4) the calculation of the susceptibility from the model. We also discuss the hyperfine fields predicted by this model.

2.1 Ionic Impurity Model

We follow Hirst[25] in development of the basic picture of the ionic impurity. The level splittings we consider, in order of decreasing size, are as follows:

(1) A balance between the Coulomb repulsion energy and the one-electron binding energy stabilizes a definite $3d^n$ configuration with splittings of about 10 eV.

(2) The Coulomb interaction splits the many-electron state into L-S terms with splittings of about 1 eV.

(3) A crystalline electric field splits the orbital states by about 0.1 eV.

(4) The spin-orbit coupling further splits the crystal-field-split orbital states by approximately 0.01 eV.

In the ionic or configuration-based approach in which we first treat H_{imp} without a mixing interaction, it is natural to assume a definite number of electrons in the impurity state. As we will discuss in more detail in Section 2.2, it is the mixing interaction which causes the impurity state to

be different from a purely definite configurational state. In Hirst's model each of the 3d impurities is assumed to be divalent, i.e., the configuration assigned to the ground state has two fewer electrons than the free atom. We start with Hirst's configurational assignment which was based on his analysis of the experimental data available at the time, but find that to explain present data it is necessary in the case of CuFe to assign the Fe impurity to a monovalent state (see Section 4.3).

The orbital angular momenta of the impurity d electrons couple together to give a many-electron orbital angular momentum $\vec{L}$; similarly the spins couple to yield a many-electron spin $\vec{S}$. The Coulomb interaction splits the various L-S terms.

The energy of an electronic orbital state localized at an atomic site within a crystal depends on its orientation with respect to the crystal due to the crystalline electric field present at the atomic site. Yafet[26] discussed the nature of the crystal field present at the site of an impurity in a Cu host and showed that it is composed of two contributions of nearly the same magnitude with opposite signs. Thus for a dilute alloy the sign of the crystal field depends crucially on the relative magnitude of the two terms.

In cubic symmetry the crystal field splits the five d one-electron orbitals into a doublet level with e_g symmetry ($3z^2 - r^2$, $x^2 - y^2$) and a triplet level with t_{2g} symmetry (xy, xz, yz). Hirst believes that the balance between the two terms leaves the triplet lower than the doublet; we find that it is necessary to assume that the doublet is the lower level in order to explain our data.

In cubic symmetry the crystal field is customarily represented by an equivalent spin-operator:[27]

$$H_{CEF} = (\Delta/120)(O_4^0 + 50O_4^4) \quad , \tag{2.1}$$

where the subscript indicates the rank and the superscript indicates the component of the spherical tensor operators. Since both contributions to the crystal field are constrained by symmetry to be of the form of Eq. 2.1, we let Δ represent the sum of both terms; its sign is determined by the larger of the two opposing terms.

The spin-orbit interaction, conventionally expressed

$$H_{so} = \lambda \vec{L} \cdot \vec{S} \quad , \tag{2.2}$$

couples the orbital and spin degrees of freedom. λ is positive for $3d^n$ configurations with n less than 5 and negative for configurations with n greater than 5.

The nature of the level structure of the many-electron, impurity state depends on the relative magnitudes of the L-S splitting, crystal field splitting and spin-orbit splitting. The spin-orbit splitting is always smaller than the L-S splitting. The three general types of structure are designated "strong," "intermediate" and "weak crystal field" depending on the size of the crystal field relative to the L-S and spin-orbit splittings. The qualitative features of the structure and their implications for measurements such as magnetic susceptibility are quite distinct. Hirst adopts the intermediate crystal field approach; we find this assumption to be consistent with our data.

The many-electron, ground state, L-S term is determined by the Hund rules:

1. First the maximum S allowed by the exclusion principle is formed;
2. The maximum value of L which is consistent with the first rule is formed.

Within the intermediate crystal field model with the doublet crystal-field-split

state lower than the triplet, the one-electron states are filled in the following order:

(1) the doublet orbital states of one spin (say spin up) are filled first;

(2) the up-spin triplet states are filled;

(3) the down-spin doublet states are filled;

(4) the down-spin triplet states are filled.

Table 2.1 gives the ground state L-S terms of the 3d configurations of immediate interest,

TABLE 2.1

$3d^n$ Ground State L-S Configurations

n	L	S
4	2	2
5	0	5/2
6	2	2
7	3	3/2

Fig. 2.1 shows how the crystal field represented by Eq. 2.1 splits the many-electron orbital states. The states given in the figure on the left are states of definite z-component of $\vec{L}$. The states with the tilde are states of fictitious angular momenta. Matrix elements of $\vec{L}$ between these states are proportional to the matrix elements between the real states; the constant of proportionality is designated by α. These states are convenient for calculation of the magnetic susceptibility as described in Section 2.4.1. For further details of the ionic structure see Ref. 27.

Figure 2.1(a): Cubic crystal field splittings of a D (L = 2) many-electron orbital state. The states given to the left are states of definite z-component $\vec{L}$. The states with the tilde are fictitious angular momentum states with constant of proportionality, α. The energy splitting is related to the crystal field operator, Eq. 2.1.

Figure 2.1(b): Cubic crystal field splittings of an F (L = 3) many-electron orbital state.

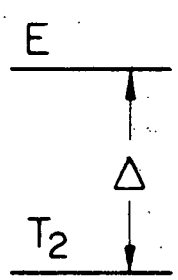

$$\frac{1}{\sqrt{2}}(|2>+|-2>) \quad |0>$$

$$\left.\begin{aligned}\frac{1}{\sqrt{2}}(|2>-|-2>) &\equiv |\tilde{0}> \\ \pm|\mp 1> &\equiv |\pm\tilde{1}>\end{aligned}\right\} \alpha = -1$$

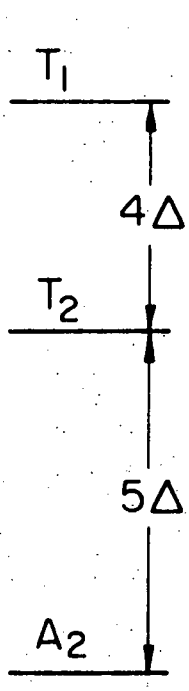

$$\left.\begin{aligned}\sqrt{\frac{3}{8}}|\pm 1> + \sqrt{\frac{5}{8}}|\mp 3> &\equiv |\pm\tilde{1}> \\ -|0> &\equiv |\tilde{0}>\end{aligned}\right\} \alpha = -\frac{3}{2}$$

$$\left.\begin{aligned}\sqrt{\frac{5}{8}}|\mp 1> - \sqrt{\frac{3}{8}}|\pm 3> &\equiv |\pm\tilde{1}> \\ \frac{1}{\sqrt{2}}(|2>+|-2>) &\equiv |\tilde{0}>\end{aligned}\right\} \alpha = +\frac{1}{2}$$

$$\frac{1}{\sqrt{2}}(|2>-|-2>)$$

2.2 Mixing Interaction

Schrieffer and Wolf[8] have shown that when the mixing interaction can be treated as a perturbation, the Anderson mixing interaction given in Eq. 1.4 taken to second order is equivalent to an interaction of the s-d form given by Eq. 1.2. Hirst[27] uses a mixing interaction of the form derived by Schrieffer and Wolf, but he allows for orbital degeneracy. He finds it convenient to use an irreducible-tensor operator notation for the purpose of calculations, but he gives a schematic form of the interaction projected onto the L-S ground state which makes the exchange form of the interaction more transparent (this form does not reveal the dependence on the wave vectors of the conduction electrons present in the tensor operator formalism):[25]

$$H_{mix} = J_S \vec{S}\cdot\vec{s} + J_L \vec{L}\cdot\vec{l} + J_{LS} \vec{L}\cdot\vec{l}\ \vec{S}\cdot\vec{s} + \ldots \quad , \tag{2.3}$$

where $\vec{L}$ and $\vec{S}$ refer to the orbital and spin angular momenta of the impurity and $\vec{l}$ and $\vec{s}$ refer to the orbital and spin angular momenta of the conduction electron. This form of the mixing interaction couples not only the spins of the impurity and conduction electrons but also the orbital angular momenta.

The mixing interaction mixes some amount of other configurations into the $3d^n$ ground state. If this mixing were strong enough, the configurational approach would be invalid or at least have to be modified. Hirst[29] states that the first non-zero term in the interconfigurational mixing is second order in the s-d form of the interaction (Eq. 2.3) and hence fourth order in terms of the Anderson one-electron mixing interaction. In the strongly magnetic alloys the mixing interaction is weak and the amount of interconfigurational mixing should be quite small. We ignore it in our treatment of the data.

The Hartree-Fock approximation to the Anderson model should be of value

for discussion of stabilization of a definite configuration since configuration stabilization is fairly insensitive to intraconfigurational details and is mainly concerned with the addition or removal of an electron from the ground state. Within the orbitally degenerate Anderson model,[6] the stabilization of a definite configuration is sensitive to the level width. If the level width is much less than the Coulomb or exchange energies, an integral number of d electrons is localized on the impurity; if the level width becomes comparable to the Coulomb and exchange splittings, the definite configuration breaks down and a non-integral number of electrons can be localized by the impurity potential. Traditionally the level width used to determine which situation obtains for the 3d impurities has been the H-F width which, as Hirst has argued, corresponds to the excited state width. If we compare the Coulomb energy to the level width of the ground state as estimated by Hirst, we expect a definite configuration even within the Anderson model.

It is the antiferromagnetic mixing interaction which is responsible for the "Kondo effect" in these alloys. (See Ref. 11 for a review of experimental aspects of the Kondo effect and Ref. 30 for a review of theoretical aspects.) As the temperature is lowered, the effective coupling strength of the interaction gradually increases until within a narrow temperature range around a particular temperature, called the "Kondo temperature," the coupling becomes effectively infinite.[31] When the coupling between the impurity moment and the conduction electrons is infinite, a further reduction of the temperature increases the polarization of the impurity moment, but the mixing produces an equal, antiferromagnetically-coupled polarization of the conduction electrons. The net effect is that below the Kondo temperature the total polarization becomes essentially temperature independent. The Kondo effect manifests itself in a number of ways, one of which being that the magnetic susceptibility

approximately obeys a Curie-Weiss law, with a Weiss temperature of the order of the Kondo temperature, rather than the Curie law of a free moment.

2.3 Spin Polarization

The mixing interaction causes some of the magnetic moment which is localized at the impurity site before the mixing perturbation is applied to "leak out" into the crystal in the neighborhood of the impurity. The mixing interaction polarizes the conduction electrons and an oscillating, damped, spin-density wave is established in the vicinity of the impurity. Thus the spin density of the conduction electrons at the host crystal sites in the vicinity of the impurity is changed from the density which exists in the pure host metal. It is the polarization of the conduction electrons at the nuclear sites which, by means of the hyperfine interaction, produces the Knight shift, K, in a metal. The Knight shift of a host nucleus which is a near neighbor of the impurity is changed from that of the pure host metal due to the presence of the spin-density wave. The change, ΔK, from the pure host Knight shift produces weak resonances called "satellites" in the tails of the "main line" resonance produced by host nuclei more distant from all impurities. In a powder each neighboring shell of nuclei will in general produce a distinct satellite. The size of ΔK for each shell, the width and intensity of the satellite resonances, and the quality of the measurement determine whether or not the satellites are resolved from the mainline and each other.

In Appendix 1 we show that

$$\frac{\Delta K}{K} = g(\vec{r})X^S(T) \quad , \tag{2.4}$$

where $X^S(T)$ is the magnetic spin susceptibility of the impurity and $g(\vec{r})$ gives the spatial dependence of the spin-density wave. The temperature dependence

of the satellite splittings is thus entirely determined by the impurity spin susceptibility. Conversely, by determining the temperature dependence of the satellite splittings, we can determine the temperature dependence of the impurity spin susceptibility.

2.4 Impurity Magnetic Susceptibility

The ground state of the impurity has a magnetic susceptibility which consists of a temperature independent contribution, plus a temperature dependent contribution that obeys a Curie-Weiss law. The concept of a temperature independent orbital susceptibility is quite familiar. It arises from admixture of a higher energy orbital state into the ground state by the applied magnetic field and gives an orbital susceptibility of order

$$\chi^{orb} \simeq \frac{\mu_B^2}{\Delta} \quad , \tag{2.5}$$

where μ_B is the Bohr magneton and Δ is the energy splitting to the excited orbital state.

A temperature independent spin susceptibility arises when the spin Zeeman coupling admixes higher states into the ground state. If the ground state wave function is a product of an orbital wave function with a spin function of definite m_s, the ground state is already an eigenstate of S_z, and there are no matrix elements of the spin Zeeman interaction between the ground and excited states. On the other hand, if the states prior to application of the magnetic field consist of a sum of products of orbital functions with states of different values of m_s, the spin Zeeman interaction will tend to change the weighting of the various m_s components in order to best take advantage of the magnetic polarization thereby induced.

When the ground state has orbital and spin angular mementa, $\vec{L}$ and $\vec{S}$,

coupled together to form a ground state angular momentum, $\vec{J}$, S_z is not a good quantum number of the states and the Zeeman interaction admixes excited states of the same $\vec{L}$ and $\vec{S}$ but different $\vec{J}$ into the ground state giving a temperature independent spin susceptibility of order

$$\chi^s \simeq \frac{\mu_B^2}{|\lambda|} \quad , \tag{2.6}$$

where λ is the spin-orbit coupling parameter. If the ground state orbital angular momentum is quenched but there is a spin-orbit multiplet of energy Δ higher due to the crystal field, one gets a temperature independent spin susceptibility of order

$$\chi^s \simeq -\frac{\mu_B^2 \lambda}{\Delta^2} \tag{2.7}$$

which should be smaller than Eq. 2.6 for reasonable crystal fields and is of the opposite sign for an atom with a positive spin-orbit coupling parameter.

In the detailed calculation of the susceptibility we first calculate the susceptibility of the impurity using the structure derived from H_{imp}. We then include the effect of H_{mix} as a perturbation. Since the highest temperature accessible experimentally is limited by the melting point of Cu to about 1300 K, and the crystal field splittings are expected to be several thousand degrees, we have limited our calculation to population of the ground state of the crystal field only. Since spin-orbit splittings are on the order of 100 degrees, we have allowed for the population of higher energy spin-orbit-split states in those cases where the ground state of the crystal field has a first-order spin-orbit splitting.

2.4.1 Susceptibility Without Mixing

The $3d^5$ configuration ground state has A_1 symmetry and no orbital

angular momentum. The first excited state is split by the L-S splitting and probably lies on the order of 10,000 K above the ground state. We ignore all but the ground state. The susceptibility is then completely spin susceptibility with a moment corresponding to S = 5/2; there is no temperature independent contribution.

$$X = \frac{g^2 \mu_B^2 S(S+1)}{3K_B T} \quad , \tag{2.8}$$

where g is the g-value of the impurity d electrons.

If the crystal field causes the states with symmetry T_2 of the orbital D state or the states with symmetry T_1 of an orbital F state to be the ground state (see Fig. 2.1), we consider the ground state of the crystal field only. We write the spin-orbit Hamiltonian

$$H_{so} = \alpha\lambda \vec{L} \cdot \vec{S} \quad , \tag{2.9}$$

relating the fictitious angular momentum operator $\tilde{L}$ to $\vec{L}$ with constant of proportionality α. The spin-orbit interaction couples $\tilde{L}$ and $\vec{S}$ together to give states of total fictitious angular momentum $\tilde{F}$ and z-component M_F. It lifts the $(2|\tilde{L}|+1)(2S+1)$ degeneracy of the ground state to give energies, $E_F = \frac{\alpha\lambda}{2} [|\tilde{F}|(|\tilde{F}|+1) - |\tilde{L}|(|\tilde{L}|+1) - S(S+1)]$. The states are

$$|FM_F\rangle = \sum_{mm'} \langle LmSm'|FM_F\rangle |LmSm'\rangle \quad , \tag{2.10}$$

where the coefficients of the states in the sum are the Clebsch-Gordan coefficients. Having treated the spin-orbit interaction exactly (within the orbital ground state), we treat the Zeeman interaction as a perturbation which mixes the states given in Eq. 2.10. We calculate the expectation of L_z and S_z for each of these mixed states and compute the thermal averages,

$\langle L_z \rangle$ and $\langle S_z \rangle$, in the usual way. The susceptibility is then derived from

$$X = - \frac{\mu_B N}{H} (\alpha k \langle L_z \rangle + 2 \langle S_z \rangle) \quad , \tag{2.11}$$

where k is the orbital reduction factor which represents a reduction of the orbital angular momentum from that of a free ion due to the crystal environment (see Ref. 27). Both the spin and orbital susceptibilities have a temperature dependent contribution and a temperature independent contribution of the form of Eq. 2.6.

If the crystal field causes the state with symmetry A_1 of an orbital F state or the states with symmetry E of an orbital D state to be the ground states, the orbital angular momentum is quenched in the ground state and no first-order spin-orbit splitting exists. In this case we treat both the spin-orbit interaction and the Zeeman interaction as perturbations to the crystal field interaction. The first-order perturbation correction to the ground state yields a temperature independent contribution to the orbital susceptibility of the form of Eq. 2.5 but no contribution to the spin susceptibility. The second-order perturbation correction to the wave function yields temperature independent contributions to both the spin and orbital susceptibilities of the form of Eq. 2.7 and a temperature dependent contribution to the orbital susceptibility.

For details on the calculation of the susceptibility for specific configurations see Appendix 2.

2.4.2. Effect of Mixing on the Susceptibility

There are two effects of the mixing which we must account for quantitatively in order to obtain reasonable agreement between the calculated susceptibility and experiment: (1) the mixing produces an antiferromagnetic

polarization of the conduction electrons and thus reduces the total experimentally measured susceptibility from that calculated in Section 2.4.1; (2) the Kondo effect causes the temperature dependence of the susceptibility to deviate from a Curie law. We treat the antiferromagnetic coupling to the conduction electrons in perturbation theory as a reduction of the effective impurity moment. We treat the Kondo effect by replacing the temperature, T, with $T + \theta$ everywhere it appears in the expressions for the susceptibility.

The experimental susceptibility of a dilute alloy is measured as the difference between the susceptibility of the alloy and that of the pure host metal; thus the experimental susceptibility includes not only the susceptibility of the impurity moment calculated as described in Section 2.4.1, but also the susceptibility of the induced conduction electron polarization. At temperatures far above the Kondo temperature the mixing interaction can be treated as a perturbation.

If the ground state angular momentum is quenched by the crystal field, only the first term in Eq. 2.3 produces a polarization of the conduction electrons $\langle s_z \rangle$ and we find

$$\langle s_z \rangle = \langle s_z \rangle_o - J_s \rho \langle S_z \rangle \quad , \tag{2.12}$$

where ρ is the density of states at the Fermi surface for one spin direction, and $\langle s_z \rangle_o$ is the polarization of the conduction electrons which would exist in the absence of the impurity (see Ref. 31). The total experimentally measured susceptibility thus takes the form

$$X_{exp} = (1 - J_s \rho) X^S + X^L \quad , \tag{2.13}$$

where X^S and X^L represent the spin and orbital susceptibilities of the

impurity respectively. It is customary to define an effective magnetic moment such that

$$X^S = \frac{\mu^2_{eff}}{3K_B T} \quad . \tag{2.14}$$

We write

$$X_{exp} = \eta^2 X^S + X^L \tag{2.15}$$

such that $\eta^2 = 1 - J_S \rho$ and η thus represents the reduction in the effective magnetic moment due to the conduction electron polarization.

If the ground state orbital angular momentum is not quenched, the form of the mixing interaction is quite complicated. To our knowledge the form of polarization induced by the general form of the mixing interaction has not been calculated. The experimental precision with which the magnetic moments of the impurities have been measured to date does not require great accuracy; therefore we make the assumption that the spin and orbital susceptibilities are affected equally because of the spin-orbit coupling and use

$$X_{exp} = \eta^2 X_{imp} \tag{2.16}$$

with

$$\eta^2 = 1 + J\rho \quad , \tag{2.17}$$

where J is now a parameter which defines the strength of the interaction. We let $J_S = -J$ in the case described by Eq. 2.15; then Eq. 2.17 suffices to describe the reduction of the magnetic moment for all cases.

Near the Kondo temperature higher order perturbation terms in the mixing become important, and in fact as the temperature approaches the Kondo temperature the coupling becomes so strong as to make perturbation theory

invalid--a calculation such as a renormalization group theory calculation is required. Krishna-murthy, Wilson and Wilkins[3] have done such a calculation using both the s-d (Eq. 1.2) and Anderson (Eq. 1.4) forms of the mixing interaction for a spin-$\frac{1}{2}$ impurity. They find that, indeed, the two forms of interaction yield identical results in the experimentally accessible temperature regime as predicted by Schrieffer and Wolf.[8] At temperatures above the Kondo temperature, they find the susceptibility can be described over any decade of temperature by a Curie-Weiss law with a moment decreased from the Curie moment. Below the Kondo temperature the susceptibility becomes constant. Although the calculation is for a spin-$\frac{1}{2}$ impurity, it explains the temperature dependence of the susceptibility of CuFe and CuMn over the entire temperature range for which it has been experimentally determined. It does not explain the temperature dependence of the susceptibility of CuCr.

We take the failure of the renormalization group calculation which included no orbital degrees of freedom, to explain the temperature dependence of the susceptibility of CuCr to be further evidence that a model with orbital structure is necessary to describe the magnetic impurities. Unfortunately, to our knowledge no calculation of even the perturbation type, other than that which we give in Appendix 1, has been done with the more complete form of mixing interaction (Eq. 2.3). Following the results of the spin-only renormalization group calculation, we compute the susceptibility by reducing the effective moment according to Eq. 2.17 and replacing T everywhere it occurs in the expression for the suceptibility with $T + \theta$. This expression yields the Curie-Weiss law behavior when only the ground state of the spin-orbit splitting is populated and passes smoothly into the proper high temperature form. We have not attempted to deduce the behavior at temperatures below the Kondo temperature.

It remains to determine the value of J to be used in calculating the

reduction of the moment (Eq. 2.17). For the spin-only case Wilson[31] gives an expression which relates the exchange coupling constant for the spin-only interaction, j, to the Kondo temperature:

$$T_K = D(\rho|j|)^{1/2} \exp(-1/\rho|j|) \quad . \tag{2.18}$$

In the spin-$\frac{1}{2}$ case, at temperatures just above the Kondo temperature the Weiss temperature in the Curie-Weiss susceptibility is $2T_K$.[3] From the observed Curie-Weiss temperature dependence we determine T_K and then use Eq. 2.18 to find j. J is roughly j times the number of orbital degrees of freedom available for the mixing interaction; thus for a completely symmetric A_1 ground state with the full orbital degeneracy of the L = 2 state, J = 5j.[6] Hirst[32] has calculated the reduction in the effective degrees of freedom which a crystal field produces. He expresses this reduction in terms of the ratio of the first order Born approximation to the resistivity, ρ_{1B}, to the second order Born approximation term which produces the Kondo effect, ρ_{2BK}. For a crystal-field-split ground state we have

$$J = 5j \times \left(\frac{\rho_{1B}}{\rho_{2BK}}\right)_{L-S} \times \left(\frac{\rho_{2BK}}{\rho_{1B}}\right)_{CEF} \quad , \tag{2.19}$$

where the subscript CEF refers to the resistivity which obtains when a crystal field is present and L-S refers to the resistivity which would exist if there were no crystal field splitting. In cases where the crystal field ground state is split by a spin-orbit coupling which is much larger than the Kondo temperature, we further reduce the expression given by Eq. 2.19 by the ratio of the degeneracy of the crystal field ground state:

$$J = 5j \times \left(\frac{\rho_{1B}}{\rho_{2BK}}\right)_{L-S} \times \left(\frac{\rho_{2BK}}{\rho_{1B}}\right) \times \frac{2F+1}{3(2S+1)} \quad . \tag{2.20}$$

For details for specific impurity cases see Appendix 2.

2.5 Hyperfine Fields

The hyperfine interaction between the impurity nucleus and the impurity electronic state may be expressed:

$$H_{hf} = g_N \mu_N \vec{I} \cdot ((H_L/L)\vec{L} + 2(H_S/2S)\vec{S}) \quad , \tag{2.21}$$

where the subscript N denotes the nucleus. We write H_{hf} in this form because the orbital and spin saturation hyperfine fields, H_L/L and $H_S/2S$, are independent of the size of the nuclear moment. Narath[33] has calculated the values of the saturation hyperfine fields expected for 3d transition metals with a Hartree-Fock approximation. In cases where enough experimental evidence exists to determine the saturation hyperfine fields from our model we compare the values deduced from the model with those of Narath's calculation; in cases where the experimental evidence is not sufficient to allow determination of both the orbital and spin saturation hyperfine fields, we use Narath's value for the orbital saturation hyperfine field, use the model to deduce the spin saturation hyperfine field from the data, and compare it with Narath's calculation. If the ground state of the impurity has zero angular momentum, the orbital hyperfine contribution vanishes (except to the extent that the Zeeman interaction causes mixing with excited states with unquenched orbital angular momentum) giving a total hyperfine saturation field:

$$H_{hf}^{sat} = 2S(H_S/2S) \quad . \tag{2.22}$$

For cases in which the ground state orbital angular momentum is not quenched, we project the hyperfine interaction onto the spin-orbit ground state:

$$H_{hf}^{sat} = -2(S_z')^{sat}(H_S/2S) - k\alpha(L_z')^{sat}(H_L/L) \quad , \tag{2.23}$$

where $(S_z')^{sat}$ and $(L_z')^{sat}$ are the effective saturated z-components of the spin and fictitious angular momentum of the spin-orbit ground state. Details for specific impurities are given in Chapter 4.

3. EXPERIMENTAL PROCEDURES

Most of the equipment and procedures used in this experiment have been described in detail elsewhere. We will give a brief description of the sample preparation, spectrometers, and data collection procedures and refer the reader to more complete discussions. Aspects which are new to this experiment are given in more detail in appendices.

3.1 Sample Preparation

The CuCr powders used in this experiment were prepared by Boyce and Stakelon as part of a general alloy preparation program which produced dilute alloys of all of the 3d transition metals in copper. Details of the sample preparation procedure are given by Boyce.[34] The samples were prepared from 99.999+% Cu rod (American Smelting and Refining Company) and 99.999% Cr lumps (United Mineral and Chemical Corporation). The Cu and Cr were heavily etched to remove surface contaminants. The appropriate proportions of Cu and Cr were placed in alumina crucibles inside quartz tubes and baked in vacuum to remove water vapor. The quartz tubes were then back-filled with 1/4 atmosphere of pure argon and sealed. After baking for one hour in an induction furnace at 1200° C, the tubes were rapidly quenched to 20° C in water. The alloys were then wrapped in 5-mil copper (99.9%) foil and swaged to less than half of their original diameter to improve homogeneity. The copper foil was removed and the surface etched away. The alloys were again sealed with argon in quartz tubes, annealed for approximately three days at 30° C to 70° C below the melting point, and then quenched in water. The surface was again etched and the alloy rod was ground to powder with a rotary grinder with a tungsten carbide cutter. For maximum penetration by the RF field, only powder which passed through a 400 mesh (less than 37 μ) sieve was used. None of the

powders were re-annealed.

Analyses of the annealed rods were made from pieces cut from both ends prior to grinding. The Cr concentrations were homogeneous to about 5%. The analyses yielded average Cr concentrations of .56, .102, .051, and .017 atomic percent for alloys which were nominally .5, .1, .05, and .01 atomic percent respectively. The .56 atomic percent alloy was examined under a microscope for macroscopic inhomogeneities. Electron microprobe analysis also showed the alloys to be homogeneous to about 5%.

3.2 Spectrometers

For historical reasons three spectrometers were used in this study. The first data obtained were taken by Aton at temperatures of 230 K and higher in a high field spectrometer with a room temperature access dewar. When he noticed an anomolous temperature dependence to the satellites, we continued the study in a low field spectrometer with a double glass dewar. With this spectrometer we were able to make measurements at liquid nitrogen (77 K), liquid neon (27 K), and liquid helium (4.2 K) temperatures. When we failed to observe the satellites at 4.2 K, it became necessary to use a cryostat which allowed operation at temperatures between 27 K and 4.2 K. The high field solenoid used for the high temperature measurements also has a cryostat dewar which allows temperature control over this temperature range; thus we inserted the cryostat into the high field solenoid and assembled a spectrometer compatible with the cryostat. All three spectrometers are hybrid-junction, bridge spectrometers. A block diagram which describes the spectrometers is shown in Figure 3.1. The RF signal from an oscillator is split; half of the power goes to the bridge and the other half goes through a variable delay line. The signal from the delay line is mixed with the signal from the bridge to

Figure 3.1: Block diagram of the spectrometers.

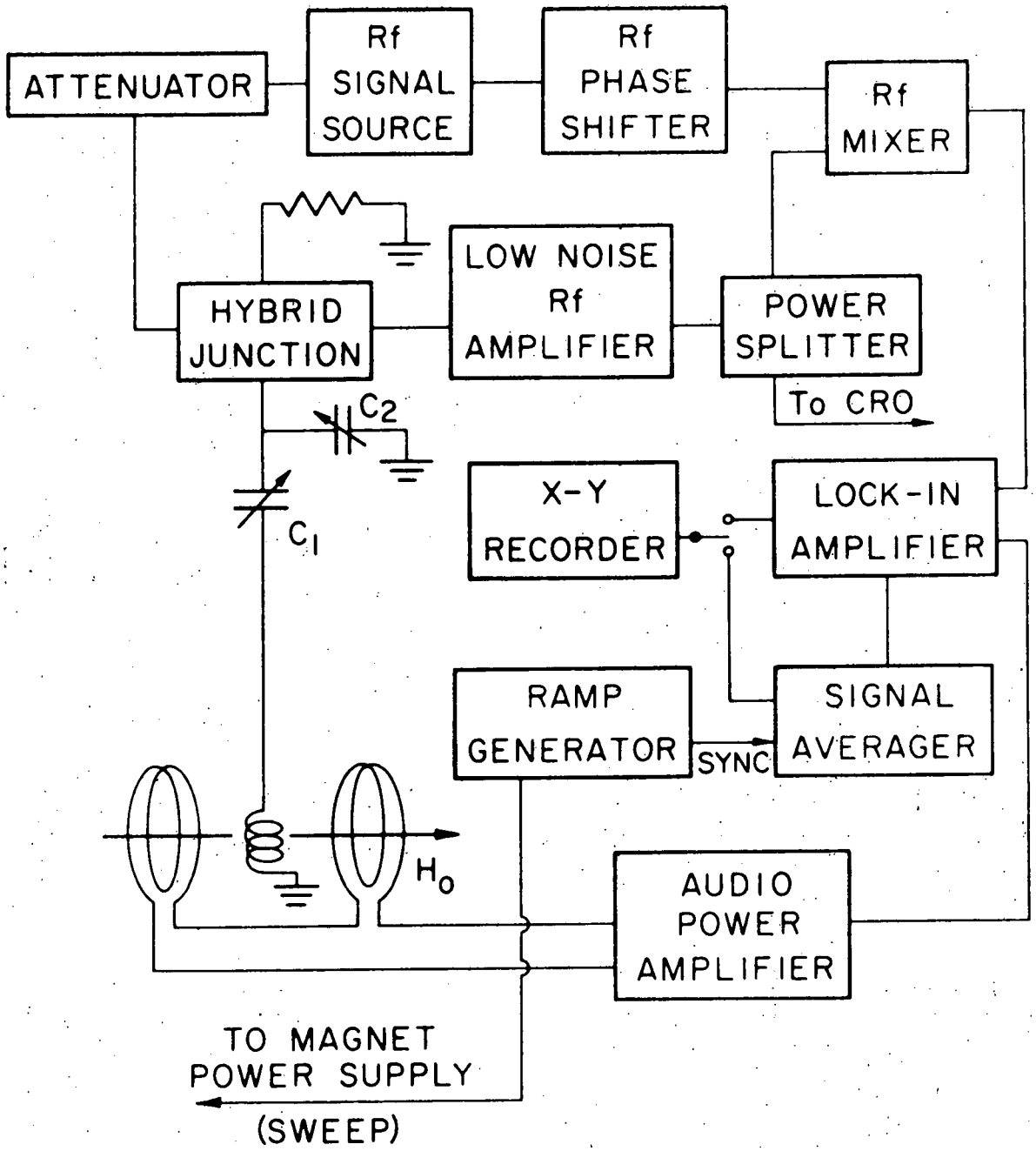
ATTENUATOR
Rf SIGNAL SOURCE
Rf PHASE SHIFTER
Rf MIXER
HYBRID JUNCTION
LOW NOISE Rf AMPLIFIER
POWER SPLITTER
To CRO
C2
C1
X-Y RECORDER
LOCK-IN AMPLIFIER
RAMP GENERATOR
SYNC
SIGNAL AVERAGER
Ho
AUDIO POWER AMPLIFIER
TO MAGNET POWER SUPPLY
(SWEEP)

allow phase sensitive detection. The RF frequency is held fixed while the magnetic field is slowly swept through the resonant field. The magnetic field is modulated with an additional small AC field and the signal is detected with a lock-in amplifier. The signal from the lock-in is usually signal-averaged to increase the signal-to-noise ratio.

Aton[18] has described in detail the spectrometer he used to obtain the high temperature data at high fields. This spectrometer incorporates a superconducting solenoid capable of producing fields up to 65 kOe. The temperature control was accomplished by passing cooling gas over the spectrometer sample probe. The equilibrium temperature of the probe was determined by a balance between the cooling effect of the gas and the heat produced by a solenoid mounted on the outside of the probe to produce the modulation field.

Follstaedt[35] has described the low field spectrometer in detail. The only significant modification we made to the spectrometer was the addition of a control circuit to maintain the amplitude of the modulation field constant. This circuit is described in detail in Appendix 3.

The electronics for the spectrometer used with the cryostat in the high field solenoid is essentially the same as that described by Aton. We added a low pass filter between the RF amplifier and power splitter to reduce higher harmonics and a low pass filter between the mixer and lock-in to avoid exceeding the dynamic range of the lock-in (see Fig. 3.1).

The sample probe arm of the spectrometer is different than that used with the room temperature access. When the room temperature access is used, the center of the solenoid is accessible from the bottom of the solenoid dewar and a probe less than half a meter in length is used. When the cryostat is used, the center of the solenoid is accessible only from the top of the dewar and a probe more than a meter long is required. At the high RF

frequencies used at room temperatures it is imperative that the probe be tuned to the bridge impedance right at the sample coil. It is difficult to tune the probe right at the sample when the sample is in a cryogenic, variable-temperature environment--the tuning condition is temperature dependent. Because it is necessary to use modest fields at low temperatures to avoid saturating the impurity moment anyway, we elected to tune the probe externally. This limited us to about 14 Mhz or about 12 kOe.

Details of the sample probe are shown in Figure 3.2. The sample is encapsulated in a nylon pill and held snugly in the RF coil by a threaded cap. The RF coil is held in the nylon probe head by two nylon screws. The end of the coaxial transmission line extends to within about two centimeters of the RF coil. Two pieces of #14 bare copper wire were soldered to the transmission line and the RF coil leads were soldered to the #14 wire. The cavity surrounding the end of the transmission line and the #14 wires was packed with Apiezon Q grease which hardens at cryogenic temperatures to provide additional rigidity. A GaAs diode used for a thermometer was mounted on one end of the RF coil form. The diode leads were held with GE 7031 varnish in a groove cut in the probe head. The diode itself was <u>not</u> attached with 7031 because 7031 attacks the diode. The diode was held in place at room temperature with dental floss and packed in Apiezon N grease which hardens at cryogenic temperatures and prevents vibrations. A copper plate attached to the outside of the transmission line forms a foot to which the probe head is attached with screws; it is electrically connected to the outer, ground conductor of the transmission line and forms a convenient grounding terminal. One lead of the diode is attached to this copper plate; the other is connected electrically to the plate by means of a 1500 pf silver-mica capacitor, which serves to attenuate stray RF signals which may be picked up by the leads from the diode to the outside

Figure 3.2: Sketch of the probe used with the cryostat in the superconducting solenoid.

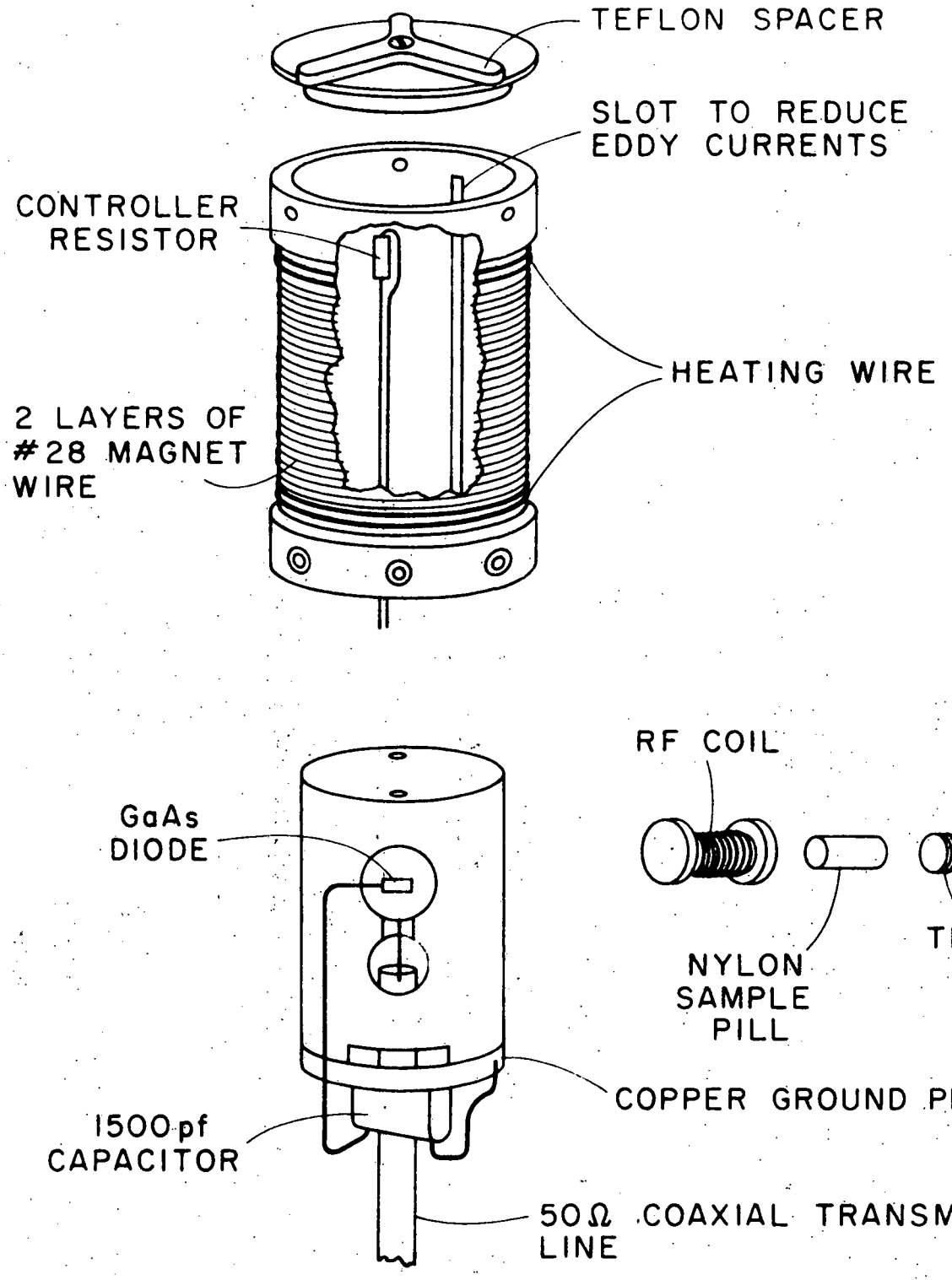
TEFLON SPACER
SLOT TO REDUCE EDDY CURRENTS
CONTROLLER RESISTOR
HEATING WIRE
2 LAYERS OF #28 MAGNET WIRE
RF COIL
GaAs DIODE
NYLON SAMPLE PILL
THREADED CAP
COPPER GROUND PLATE
1500 pf CAPACITOR
50 Ω COAXIAL TRANSMISSION LINE

of the solenoid dewar. A 1/8-in. thick brass can with a brass lid and a teflon spacer fits over the probe head. This can serves several purposes: (1) it is an RF ground shield to prevent stray pickup in the RF coil; (2) it provides support for the modulation solenoid which is wound around it; (3) it represents a large thermal mass which helps to maintain the sample at constant temperature. The thickness of the can is the result of a trade off. The thicker the can, the better thermal mass it provides; however the thicker the can, the more it also attenuates the modulation field which reaches the sample. A 1/16-in. wide slot cut to within about 1/4 in. of each end of the can reduces the eddy current flow which the modulation field induces in the can and thus helps to reduce the attentuation of the modulation field. The modulation solenoid consists of two layers of #28 magnet wire insulated from the can and each other by layers of 1/2-mil mylar and coats of 7031. It is imperative to insulate the modulation coil from the can because if the modulation coil is grounded at the probe, a relatively large audio signal will usually ride on the RF ground and produce a large offset at the lock-in. A length of Advance heating wire with 30 ohms resistance is wound bifilarly at both ends of the can; this length allows two turns at one end and three at the other. We wound the three turns on the lower end of the can which is closest to the helium gas valve used for cooling. On the inside of the can, right behind the three turns of heating wire is a 1/8-watt, 560-ohm, Allen Bradley resistor which is used as the temperature sensor for the temperature controller. The resistor is insulated from the can electrically but kept in good thermal contact by a piece of cigarette paper and 7031. The resistor leads are protected from stray RF pickup with a 1500-pf capacitor shunt similar to that used on the GaAs diode. The leads from the diode, modulation coil, heating wire, and resistor are secured at the probe head with dental floss and 7031;

they are taped to the outside of the transmission line and pass out of the solenoid dewar through insulating connectors. The transmission line, which was made by Stakelon, is copper-plated stainless steel with air dielectric and nylon spacers. The probe end of the transmission line is sealed with Stycast 2850GT to prevent helium from entering the line and changing its impedance. Unfortunately Stycast 2850GT has alumina filler and the Al^{27} NMR from the Stycast produces a signal about the same size as the satellites and causes some interference. Six polished aluminum radiation shields are spaced along the length of the transmission line.

3.3 Temperature Control and Measurement

Temperature control in a magnetic resonance experiment at temperatures of a few degrees Kelvin causes a problem. Ideally one would like to have the sample, thermometer, heating element and controller temperature sensor all in excellent thermal contact. To prevent stray RF pickup the heating element with its relatively large currents must be kept electrically isolated from the RF coil. These two constraints require that the material separating the sample and the heating element be a poor electrical conductor but a good thermal conductor at these temperatures. For handling the material must be rigid at room temperature. The only material of which we are aware that meets these criteria is solid sapphire. Besides being expensive, sapphire has an Al^{27} NMR which would swamp the weak satellite signals.

We have adopted a compromise approach to the temperature control problem. The temperature of a large thermal mass (the brass can and lid and the copper foot) which surrounds the sample is controlled. Good thermal contact is established between the thermal mass, heating element, and controller temperature sensor, but a temperature gradient is allowed to develop between the

thermal mass and the sample. A thermometer which requires only a small DC current and is protected from stray RF is placed in thermal contact with the sample. With the thermal mass, heating element, and controller temperature sensor in good thermal contact the temperature of the thermal mass can be controlled very stably. The poor thermal contact between the thermal mass and the sample means that it may take the system a while to come to equilibrium, but once equilibrium is reached the tamperature of the sample should be nearly as stable as that of the thermal mass. The sample temperature can be read accurately with the thermometer because they are in good thermal contact.

An Artronix Model 5301-E temperature controller was used. This unit uses a potentiometer bridge circuit to sense the voltage across a temperature sensitive device. It also has its own constant current source to supply resistive devices. A 1/8-watt, 560-ohm, Allen Bradley resistor was chosen as the temperature sensor because it is inexpensive, readily available, and has a good temperature coefficient over the range of 4.2 K to about 30 K. The resistor is also less sensitive to magnetic fields than most other devices used for low temperature thermometry.[36]

The cryostat used with the superconducting solenoid is a Janis Vari-Temp Dewar. It has a capillary from the solenoid helium chamber to the sample chamber. Helium flow through the capillary is controlled by a needle valve. A heater which contacts the capillary allows the helium to be vaporized. The cooling capacity of the gas can be varied by adjusting the needle valve and the heater current. The gas flow was monitored with a flow meter. Four user-controlled variables contribute to the temperature equilibrium of the sample: (1) the helium flow rate, (2) the gas heater current, (3) the heating effect

of the modulation field current, and (4) the heat supplied by the controller. With practice it is possible to cool down from liquid nitrogen temperature and reach equilibrium at the desired temperature within half an hour. Once at equilibrium the temperature can be maintained to with ±0.2 K for a period of at least two hours, the longest time for which continuous signal averaging was attempted while at a controlled temperature.

Since the thermometer was to be placed right next to the RF coil, it had to be a low current, DC activated device or a thermocouple. We wanted to be able to read the temperature accurately to 0.1 K. The device had to withstand temperature cycling while maintaining its calibration. It would be preferable if it was relatively insensitive to magnetic fields. We also preferred to use one thermometer with reasonable sensitivity over the entire temperature range of 4.2 K to 300 K. These criteria narrowed our choice to a GaAs diode or a AuFe thermocouple.[36,37] With the help of P. Anthony we calibrated a Au-.07 at% Fe-KP thermocouple and a GaAs diode (Scientific Instruments Model GA-300, SN 90251) from 4.210 K to 96.4 K. The calibration was done in A. C. Anderson's cryostat using his Ge resistor thermometer (4182-R) as a secondary standard. The diode was calibrated with a four lead configuration and the voltages were read on a 10^{10} ohm input impedance DVM which was first checked for calibration against a standard cell. A home-built constant current source consisting of a 741 operational amplifier with a mercury reference cell provides 10 μA to the diode. Thermal cycling to room temperature and back down to 10 K revealed that the diode maintained its calibration to within the accuracy with which the voltage was read (0.1 K); the calibration of the thermocouple changed by about 0.3 K. We used the diode for our thermometer. During our data collection a Leeds and Northrup 755 type K-5 guarded potentiometer was used with a null detector to measure the diode voltage. The

temperature was easily read to an accuracy of better than 0.1 K. A slight sensitivity to magnetic fields (an error of +0.1 K at 10 kOe followed by a drop to an error of -0.9 K at 55 kOe) was measured at 4.2 K and corrected for.

Although they produced no useable data, several runs were made at temperatures from 1.5 K to 4.2 K. In this range the temperature was controlled by maintaining a constant helium vapor pressure with a manostat. The temperature was measured by reading the vapor pressure on a Wallace and Tiernan gauge (0.1 - 20 mm, 0 - 100 mm, and 0 - 400 mm). This proved to be an extremely stable way to maintain the temperature.

3.4 Data Collection

The mechanics of adjusting and optimizing the spectrometer for observation of a particular resonance are given in detail by Follstaedt.[35] In summary, the magnetic field is swept through the resonant field slowly enough to avoid line shape distortion. The field sweep speed and time constant of the lock-in amplifier are coordinated so that the desired number of time constants are spent during the time the field is sweeping through the resonance. The modulation field amplitude and frequency are optimized subject to the trade offs discussed below. The modulation frequency is always chosen low enough to avoid line shape distortion. The amplitude of the RF field is adjusted to optimize the signal-to-noise ratio.

The parameter, ΔK, which is proportional to the impurity spin susceptibility, is determined from the difference in the resonant fields of the Cu main line and the satellites. The low pass filter in the lock-in which attenuates high frequency noise also attenuates the high frequency components of the signal; a trade off must be made between signal-to-noise ratio and

signal distortion. The first effect of signal distortion is a shift in the apparent resonant position. The amount of shift is determined by the number of time constants spent sweeping through the line. Because the satellites are much broader than the main line at low temperatures, the low pass filter shifts the resonances by different amounts. Traditionally, accurate determination of ΔK has been made by sacrificing signal-to-noise and spending enough time sweeping through the resonance to ensure that the main line and satellites are shifted by nearly the same amount (enough of the high frequency components are kept to avoid serious distortion). We have analyzed the problem of line shape distortion by a low pass filter and developed a technique which allows correction for the apparent shift in resonant position even when the resonance has been shifted significantly by choosing the time constant long enough to optimize the signal-to-noise. The accuracy of the technique was verified experimentally. This technique allows a reduction of 30 to 50% in the required averaging time. Details of this technique are given in Appendix 4.

Selection of the modulation field amplitude involves a trade off similar to that of the selection of the time constant. The maximum signal is achieved with the peak-to-peak modulation amplitude equal to twice the peak-to-peak line width (for the derivative of the absorption signal) or greater depending on the line shape. Such a large amplitude produces significant line shape distortion. (See Ref. 38 for discussion of modulation effects.) When searching for a resonance whose position was unknown, we used a modulation amplitude about twice the expected line width. When the resonant position was known, the amplitude was limited to half the line width to reduce distortion. A technique which allows the correction of distortion caused by large modulation amplitude, described by Wind and Emid,[39] was implemented and

tested but not used in collection of this data for lack of digital processing equipment. This digital technique allows data to be collected with a modulation amplitude equal to the line width and reduces the distortion to a level comparable with that produced by a modulation amplitude of half the line width; the result is a reduction of about 50% in the required signal averaging time.

Experimental design constraints often limited the frequency and amplitude of the modulation to much less than the optimum determined on the basis of signal-to-noise and distortion considerations alone. It was found that the frequency and amplitude of modulation often had to be reduced to avoid excessive offset drift at the lock-in. Apparently the eddy currents induced by the modulation field in the brass can, flowing in the magnetic field, produce vibrations whose amplitudes are not constant. In practice a trade off had to be made between the increase in signal and increase in offset drift produced by increased modulation amplitude, and another trade off was made between the decrease in high frequency noise and the increase in offset drift produced by an increased modulation frequency.

Four different impurity concentrations were used to verify the concentration independence of the satellite splittings and to optimize the experimental resolution of the satellites over the wide temperature range. At low temperatures the satellites become broader and more difficult to resolve; it is often easier to resolve the satellites in more dilute samples. The fields used in the experiment ranged from 5 to 55 kOe. At high temperatures a large field is necessary to split the satellites enough to resolve them; at low temperatures the splittings are larger and a lower field is advantageous. It is also important at low temperatures to use a field small enough to avoid saturation of the impurity moment, i.e., we want to measure the susceptibility in a field

small enough that the susceptibility is essentially field independent. Table 3.1 shows the samples and field strengths used at the various temperatures at which data were taken. No concentration or field dependence was observed.

Cu has two isotopes with magnetic moments--Cu^{63} and Cu^{65}. We verified that the satellite resonances are present for both Cu isotopes, thus confirming that the resonances we attribute to Cu nuclei which are neighbors of the Cr impurity are indeed Cu resonances and not the spurious resonances of some other nuclei.

TABLE 3.1

Impurity Concentrations and Field Strengths

The field strengths used at each temperature are given. The samples investigated are indicated by an x.

T (K)	Concentration (at%) .56	.102	.051	.017	Field (kOe)
334		x			
278	x	x			55
230		x			
77		x	x		10 to 23
27.1			x		10
15.1			x	x	12
8.0			x		
4.2			x	x	
3.0			x		5 to 12
2.5			x		
1.4			x		

4. COMPARISON OF DATA WITH THEORY

In this chapter we give the results of our NMR satellite measurements on CuCr and show that they are explained by the model developed in Chapter 2. Using published CuCr bulk magnetic susceptibility data, we further substantiate the model. We discuss the observed anomolous behavior of the low temperature susceptibility in terms of the model and the impurity hyperfine fields calculated from the model. Using NMR satellite, bulk susceptibility, and impurity hyperfine field data available on CuMn and CuFe we extend the model comparison and find substantial improvement in the understanding of all three alloys over that afforded by previously published models.

4.1 CuCr

In this section we give the results of the CuCr satellite measurements and show that they can be explained by the model developed in Chapter 2. Using no additional adjustable parameters, we calculate the bulk susceptibility from the model. We discuss the published bulk susceptibility data and show that the data are explained by the model to within the experimental uncertainties. After a reinterpretation of one of the bulk susceptibility experiments, we find good agreement between the model and the data over the entire temperature range of 12 K to 700 K. We discuss the anomolous temperature dependence of the bulk susceptibility observed at room temperatures less than 10 K in terms of the model. Finally, we calculate the Cr hyperfine fields from the model and compare them with those observed experimentally.

4.1.1 NMR Satellite Data

The NMR satellite data obtained in this investigation are displayed in Fig. 4.1. Since $\Delta K/K$ is proportional to the impurity spin susceptibility (see Eq. 2.4), we have plotted $K/\Delta K$ versus the temperature; on such a plot a

Figure 4.1: A plot of the CuCr satellite data. The dashed lines represent a Curie-Weiss law fit to the low temperature data. The solid lines are the fit to the model described in the text.

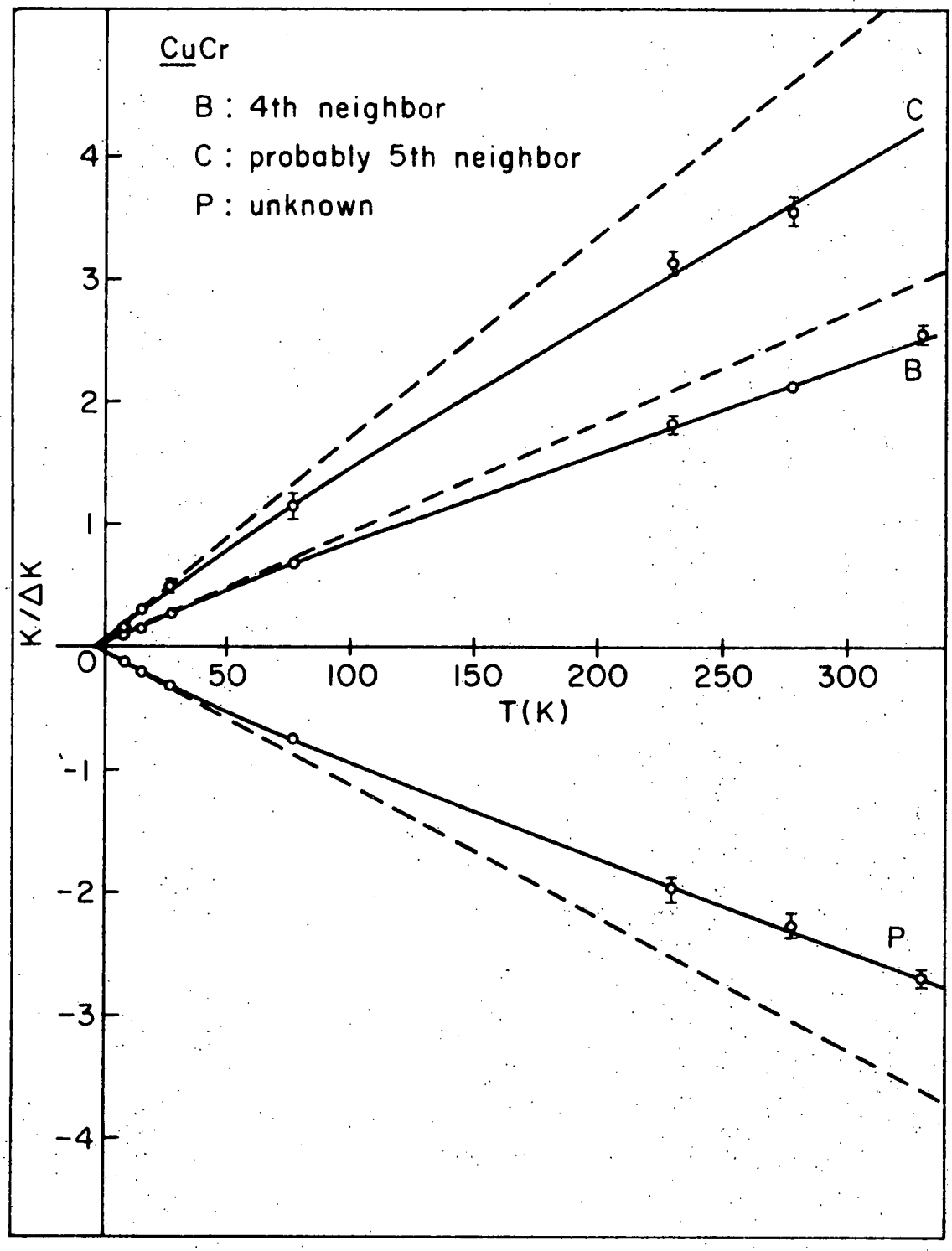
CuCr
B : 4th neighbor
C : probably 5th neighbor
P : unknown
C
B
P
K/ΔK
T(K)
4
3
2
1
0
-1
-2
-3
-4
50
100
150
200
250
300

Curie-Weiss law appears as a straight line which intercepts the abscissa at the negative of the Weiss temperature. The dashed lines are straight lines drawn through the low temperature data; the uncertainties of the low temperature data are sufficiently small to require the slopes shown. The data deviate by about 20% from the Curie-Weiss law at 300 K. It is fortunate that the satellite labeled "P" is shifted to the opposite side of the main line from B and C. Because all three satellites are shifted closer to the abscissa (further from the main line) than the Curie-Weiss law predicts, we know that the deviation is not due to a shift in the main line resonance caused by some experimental error.

If we assume that the impurity spin susceptibility is given by the sum of a Curie-Weiss term and a temperature independent term, the shift of satellites is given by

$$\left.\frac{\Delta K}{K}\right)_s = C_s \left(\frac{1}{T+\theta} + C\right) \quad , \tag{4.1}$$

where C_s is a constant of proportionality which is different for each satellite and is determined by the spatial dependence of the spin density oscillation surrounding the impurity (see Eq. 2.4). A computer fit of the data to Eq. 4.1 produces a reasonably good fit with $\theta = 4.0 \pm .6$ K and $C = (7.4 \pm 2.4) \times 10^{-4}$ K^{-1}. To demonstrate the fit we subtract CC_s from both sides of Eq. 4.1 and plot the inverse versus temperature in Fig. 4.2. If Eq. 4.1 is correct, the result should be a straight line. The fit indicates that there is a temperature independent contribution to the spin susceptibility of the Cr.

As we discussed in Section 2.4, a temperature independent contribution to the impurity susceptibility indicates that the impurity has excited states. The detailed atomic level structure of the Cr impurity appears to be

Figure 4.2: A fit to the CuCr satellite data assuming that the impurity spin susceptibility is given by the sum of a Curie-Weiss term and a temperature independent term.

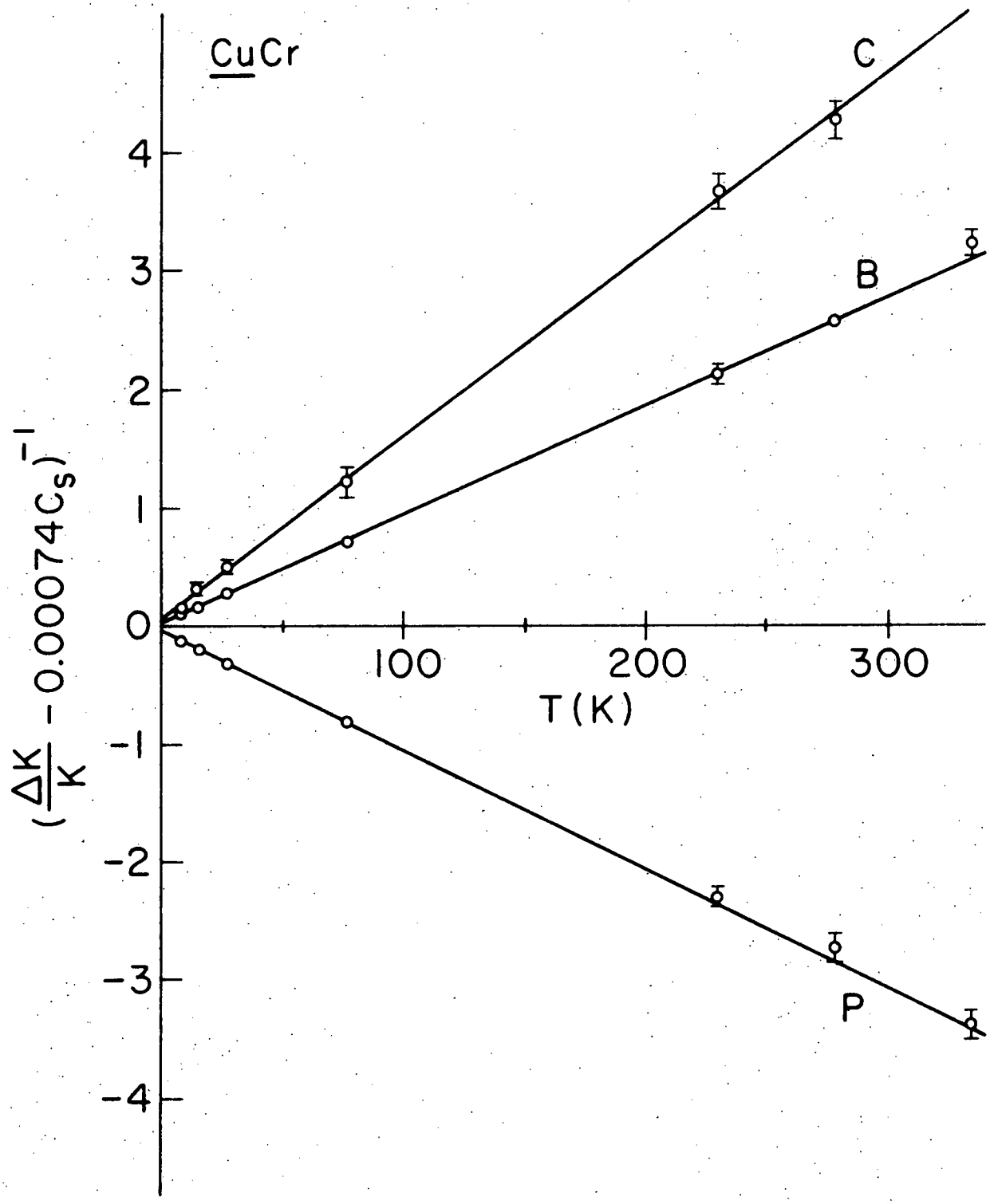
CuCr
C
B
P
4
3
2
1
0
-1
-2
-3
-4
100
200
300
T(K)
$(\frac{\Delta K}{K} - 0.00074 C_s)^{-1}$

manifesting itself, contrary to the assumption in some models that the impurity structure is broken down by the impurity electron-conduction electron mixing interaction. Present calculations made from the Anderson model seem to be inadequate to treat CuCr because they do not include the detailed atomic structure.

We compare the data with the model developed in Chapter 2 which first treats the impurity structure in detail and then treats the mixing interaction as a perturbation. Following Hirst we first attempt a fit to the $3d^4$, E symmetry ground state which results if the t_{2g} symmetry single-electron orbitals have lower energy than those with e_g symmetry. From Appendix 2 we have for the spin susceptibility:

$$\chi^S = 8\mu_B^2 N\left[\frac{1}{K_B T} - \frac{2\lambda k}{\Delta^2}\right] \quad . \tag{4.2}$$

A Cr^{++} ion ($3d^4$) has a spin-orbit coupling, λ, of +58 cm^{-1},[27] and therefore the temperature independent term in Eq. 4.2 is negative while the fit to the satellite data indicates a positive temperature independent term; thus Hirst's assignment of the ground state does not explain the satellite data.

Comparison of the experimental evidence on CuCr and CuFe gives a clue as to what is happening. Both CuCr[13,40] and CuFe[14] have a temperature independent contribution to their bulk magnetic susceptibility; but although the CuCr satellite data show a 20% temperature independent contribution to $\Delta K/K$ at 300 K, no temperature independent contribution to the satellite data is observed for CuFe to within the experimental uncertainties.[19,20] The indication is that the ground state of Cr has an unquenched orbital angular momentum with a temperature independent contribution to the spin susceptibility of the form of Eq. 2.6 while the ground state of Fe has its orbital angular momentum

quenched and a temperature independent contribution to its spin susceptibility like Eq. 2.7 which is expected to be smaller than that of Eq. 2.6. If the t_{2g} symmetry single-electron orbitals are lower than those with e_g symmetry as Hirst suggests, the $3d^4$ configuration has an E symmetry ground state with quenched orbital angular momentum and the $3d^6$ (Fe^{++}) and $3d^7$ (Fe^{+}) configurations have T_2 and T_1 symmetries respectively with unquenched orbital angular momentum. This assignment disagrees with the conclusion made from the bulk susceptibility and satellite data. If the sign of the crystal field is opposite of that assumed by Hirst so that the e_g symmetry single-electron orbitals have lower energy than those with t_{2g} symmetry, the $3d^4$ configuration ground state has T_2 symmetry with unquenched orbital angular momentum and the $3d^6$ and $3d^7$ configurations have E and A_2 symmetries respectively with quenched orbital angular momentum; thus by assuming the sign of the crystal field opposite of that usually proposed, we can qualitatively account for the experimental evidence on CuCr and CuFe. In the following discussion we attempt to make the agreement quantitative.

If the crystal field causes the e_g single-electron orbitals to have lower energy than the t_{2g} symmetry orbitals, the 3d atomic level structure is that shown in Fig. 2.1(a). The ground state has T_2 symmetry with fictitious angular momentum, $|\tilde{L}| = 1$. The spin-orbit interaction couples the orbital and spin states ($S = 2$) to give states of total fictitious angular momentum, $\tilde{F}$. The resultant level structure is shown in Fig. 4.3. Note that only first-order spin-orbit splittings are shown. Higher order spin-orbit terms split the remaining degeneracies down to the degeneracies required by symmetry. These higher order splittings, except those in the $F = 3$ ground state where the splittings can become of the order of the temperature or greater, are unimportant for calculation of the susceptibility. We ignore the higher order

Figure 4.3: The level structure of Cr^{++} showing the effect of the crystal field and first-order spin-orbit coupling. The numbers in parentheses indicate the degeneracies of the levels.

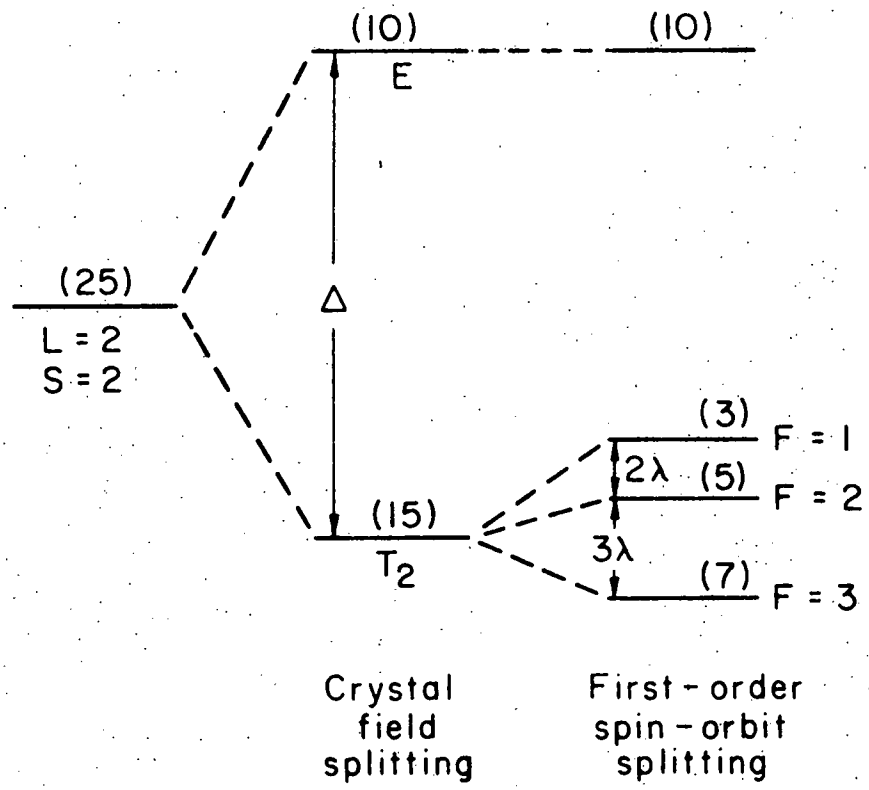
(10)
(10)
E
(25)
L = 2
S = 2
Δ
(3)
F = 1
2λ
(5)
F = 2
(15)
T2
3λ
(7)
F = 3
Crystal field splitting
First - order spin - orbit splitting

splittings for the moment and will discuss them further when we discuss the low temperature bulk susceptibility data.

As discussed in Section 2.4.1, the crystal field splitting is expected to be several thousand degrees; we ignore the excited crystal-field-split E symmetry states. Since the spin-orbit coupling parameter in Cr^{++} is 84 K, we include all of the spin-orbit-split T_2 states. Each spin-orbit-split level has a Curie-Weiss law contribution to the susceptibility plus a temperature independent contribution that results from mixing of the spin-orbit-split states by the Zeeman interaction. Thus the susceptibility of the Cr arises primarily from the F = 3 ground state with some contribution from the excited F = 2 and F = 1 states at the higher temperatures. The full expression for the spin susceptibility is given in Appendix 2. A computer fit to the satellite data, allowing the Weiss temperature, spin-orbit coupling parameter, and the orbital reduction factor to be free parameters, yields the fit shown in Fig. 4.1 and tabulated in Table 4.1 with θ = 2.9 ±1.0 K, λ = 48 ±32 cm^{-1}, and k = 0.84 ±.19. The normalized chi-square of this fit to the data is 0.56, somewhat better than the chi-square value of 0.70 obtained for the fit shown in Fig. 4.2 which included only one Curie-Weiss term and one temperature independent term. The orbital angular momentum and spin-orbit coupling are both reduced to about 80% of the free ion values. Such a reduction is to be expected and is of a reasonable magnitude.[27] The large uncertainty in the determination of the parameters is due to the strong interdependence of the parameters. The uncertainties quoted are the amount of change necessary in a given parameter to change the normalized chi-square of the computed fit by 1.

The fit shown in Fig. 4.1 and tabulated in Table 4.1, based on the assumption that the satellite splittings are proportional to the impurity spin susceptibility only, appears to explain the data quite well. We also tested

TABLE 4.1

Fit of Model to CuCr NMR Satellite Data

The NMR data are compared with the model calculation for satellites B, C and P. The experimental uncertainties are given in parentheses.

T (K)	$(\Delta K/K)_B$		$(\Delta K/K)_C$		$(\Delta K/K)_P$	
	exp	calc	exp	calc	exp	calc
334	.39 (1)	.396			- .37(1)	- .363
278	.469(7)	.469	.281(9)	.276	- .44(2)	- .430
230	.55 (2)	.558	.32 (1)	.328	- .51(2)	- .511
77	1.48 (6)	1.45	.87 (8)	.851	- 1.31(6)	- 1.33
27.1	3.58 (8)	3.54	2.0 (2)	2.08	- 3.2 (1)	- 3.24
15.1	6.1 (4)	5.76	3.1 (4)	3.38	- 5.0 (3)	- 5.27
8.0	9.1 (6)	9.38	5.8 (3)	5.51	- 8.5 (5)	- 8.59

the hypothesis that the splittings are proportional to the total impurity susceptibility. (See the formula for the susceptibility in Appendix 2.) The fit thus obtained is not as good as the fit to the spin susceptibility only; furthermore the value of the spin-orbit parameter required to produce the fit is 350 ±160 cm^{-1} and the magnetic moment obtained from the fit is 3.2 μ_B. The experimental value for the moment is 3.7 ±0.4 μ_B (see the following section). The Cr^{++} free ion has a spin-orbit coupling parameter of 58 cm^{-1}. The spin-orbit interaction is expected to be reduced slightly in the metal host--certainly not increased by a factor of six. We conclude that the fit to the total susceptibility is unphysical while the fit to the spin susceptibility gives empirical evidence that the satellite splittings are proportional to the spin susceptibility only and thus Eq. 2.4 is correct.

4.1.2 Bulk Magnetic Susceptibility Data

Due to the spin-orbit coupling the spin and orbital susceptibilities are not independent; the determination of the model parameters from the satellite data allows calculation of the bulk susceptibility. The only additional factor required is η^2, the mixing reduction parameter, which is calculated from Eq. 2.20. The complete expression for the susceptibility is given in Appendix 2. The calculated susceptibility is plotted versus $1/(T + 2.9)$ in Fig. 4.4. Note that since the first excited spin-orbit-split state lies approximately 200 K above the ground state, the susceptibility becomes essentially a Curie-Weiss law plus a temperature independent term below about 100 K. Since the spin-orbit splittings become unimportant at temperatures much greater than the total spin-orbit splitting (the sum of the temperature independent terms of the three spin-orbit split levels is zero), the temperature independent term vanishes and the susceptibility approaches zero at infinite temperatures.

(Of course we have ignored the excited crystal field states which would contribute at temperatures of a few thousand degrees, but the experimental data are limited to temperatures lower than 700 K.) The Weiss temperature is assumed to be the same as that determined from the satellite data since the spin and orbit are coupled; the total effective magnetic moment in the low temperature regime is calculated to be 3.4 ±0.4 μ_B.

Monod and Schultz[41] measured the bulk magnetic susceptibility of a 36 ppm CuCr sample over the temperature range of 1.5 K to 25 K. They did not show their data, but they reported that they fit the data to a Curie-Weiss law with a Weiss temperature of 1.0 ±0.5 K and an effective magnetic moment of 3.94 ±0.13 μ_B. They measured the susceptibility for only one sample and assumed that the susceptibility was proportional to the Cr concentration. Because these results differ significantly from a more recent and apparently more thorough experiment, we have chosen to use only the more recent data.

Vochten, Labro and Vynckier[13] have reported a bulk susceptibility study of CuCr on three samples with 5 ppm, 15 ppm, and 112 ppm atomic concentrations of Cr at temperatures from 1.5 K to 300 K and fields from 3.96 kOe to 12.64 kOe. The susceptibility of the 5 ppm Cr sample was plotted versus the susceptibility of the 15 ppm Cr sample for all temperatures and fields. The fact that all the data fall on a straight line is strong evidence that the susceptibility measured is the susceptibility of isolated impurities only. A similar plot for the 112 ppm Cr sample versus the 15 ppm sample shows some deviation from a straight line for the low temperature data; this deviation is attributed to cluster effects in the 112 ppm Cr sample. Vochten et al. use the ratio of the susceptibilities measured in the two most dilute samples to that measured in the 112 ppm sample to establish "more precise concentrations" for those samples--henceforth using 4.13 ppm and 12.7 ppm as the concentrations

Figure 4.4: The bulk magnetic susceptibility of CuCr. The curve is the susceptibility calculated from the model described in the text. The open circles are a representation of the experimental data of Hoeve and Van Ostenburg, and Vochten, Labro and Vynckier as described in the text.

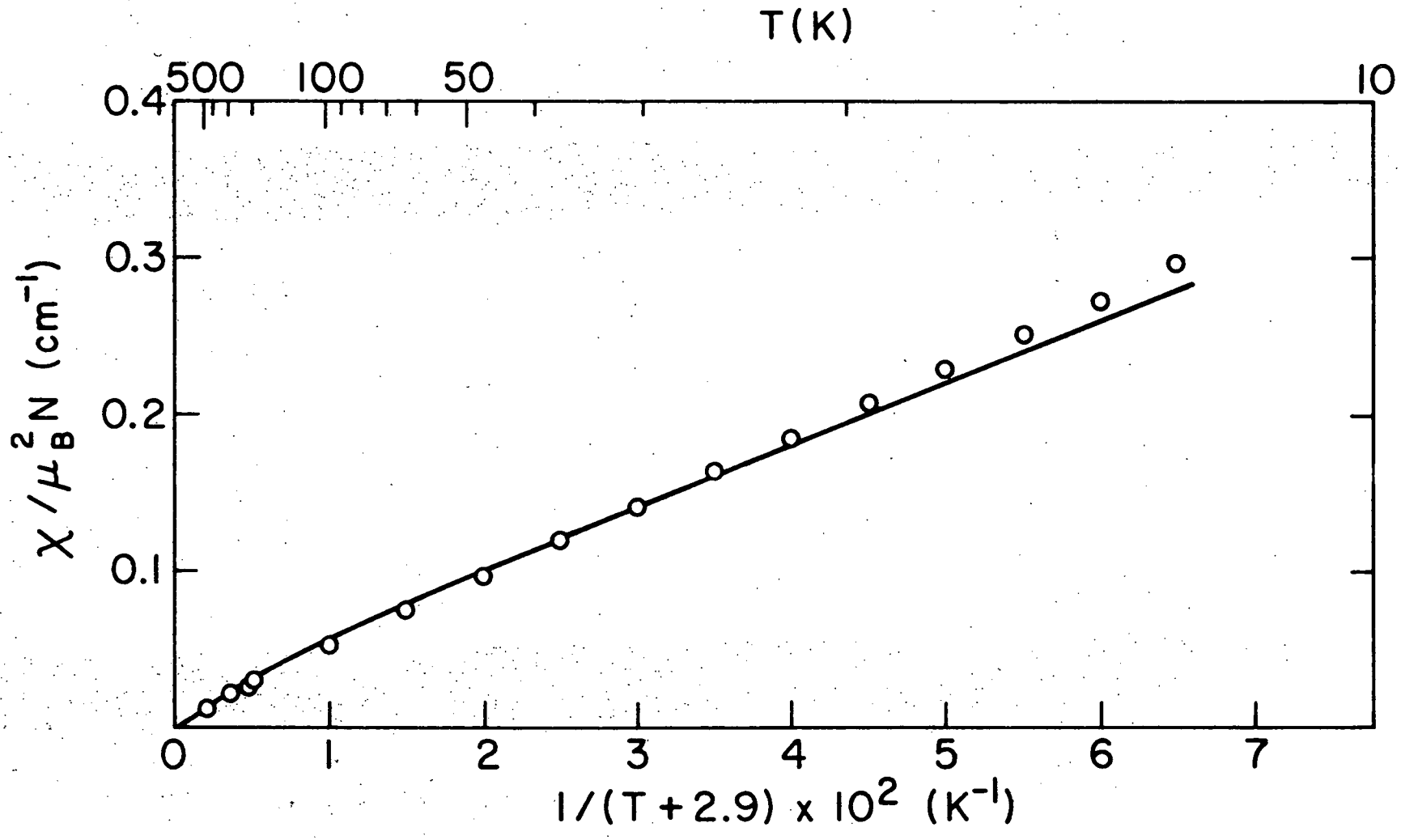
T(K)
500
100
50
10
0.4
0.3
0.2
0.1
0
1
2
3
4
5
6
7
$\chi/\mu_B^2 N$ (cm^{-1})
$1/(T+2.9) \times 10^2$ (K^{-1})

of those samples. We shall focus on the data from the 15 ppm sample as it appears to be free from cluster effects and gives essentially the same results as the 5 ppm sample with the exception of better precision, presumably due to stronger signals. Vochten et al. show their susceptibility data only as a function of 1/T which makes it impossible to determine the high temperature data, but they claim to be able to fit the data from 300 K down to 12 K with the sum of a Curie-Weiss term and a temperature independent term and quote a Weiss temperature of 3.4 ±.3 K and an effective magnetic moment of 3.99 ±.04 μ_B. The Weiss temperature and moment are both somewhat higher than the values calculated from the model, but they fall within the uncertainties of the calculation.

Although the model calculation gives fair agreement with the data as analyzed by Vochten et al., reinterpretation of the data in a manner we feel to be more nearly correct improves the agreement. We find two points of disagreement with the published interpretation: (1) we feel the experimental uncertainties have been vastly understated, and (2) we take issue with the determination of more precise impurity concentrations for the two most dilute alloys by scaling the susceptibilities.

Since the impurity susceptibility is proportional to the number of impurity atoms contributing to the susceptibility, determination of the effective magnetic moment is limited by the precision to which the concentration of isolated impurities is known. Since Vochten et al. were willing to adjust the impurity concentrations by 16% with their scaling procedure, we argue that the uncertainty in the determination of the impurity concentration may be as high as 16% (Vochten et al. give no uncertainties for their concentration analysis). A 16% error in the concentration results in an 8% error in the determination of the effective magnetic moment. The uncertainties quoted

for the susceptibility parameters appear to reflect only the uncertainties due to data scatter, as is further evidenced by the fact that the size of the temperature independent contributions to the susceptibilities quoted for the three samples are by no means proportional to the concentrations to within the uncertainties quoted. The strong interdependence between the parameters in a fitting procedure also seems to have been neglected in stating the uncertainties. An error in determination of the Weiss temperature, for example, strongly affects the value determined for the moment since the low temperature data is implicitly weighted strongly in a fit to a Curie-Weiss law.

The scaling procedure used to determine the impurity concentration in the more dilute alloys tacitly assumes that the analyzed concentration of the 112 ppm sample is all in the form of isolated impurities--despite the experimental evidence that the 112 ppm sample does suffer from clustering. We view the fact that the percentages by which the concentrations of the more dilute alloys were scaled are nearly the same (-15% and -17%) as further evidence that a more nearly correct interpretation of the data is that the 112 ppm sample has about 16% of its impurity concentration in the form of clusters. In any event, the possibility of this alternate interpretation means that the moment determined by the experiment is subject to considerable uncertainty.

In view of these objections to the analysis of the bulk susceptibility data, we have reanalyzed the data assuming the concentration of the "12.7 ppm" alloy is 15 ppm. The effective magnetic moment is then $3.7 \pm 0.4\ \mu_B$, where the uncertainty is only our estimation as to the minimum experimental uncertainty reflected by the data. We have plotted the rough form of the data on Fig. 4.4 by using the expression derived from our analysis of this experiment, given as Eq. 4.3 below, for the susceptibility for 12 K to 300 K and the

expression given as Eq. 4.4 below, derived from analysis of published data obtained in a separate experiment by Hoeve and Van Ostenburg[40] at higher temperatures, for the temperature range of 300 K to 700 K. The expressions used for the susceptibility are

$$X = \frac{(3.67)^2 \mu_B^2 N}{3K_B} \left(\frac{1}{T+3.4} + 12.4 \times 10^{-4} \right) \quad ; \tag{4.3}$$

$$X = \frac{(4.00)^2 \mu_B^2 N}{3K_B} \left(\frac{1}{T+2.9} + 3.6 \times 10^{-4} \right) \quad . \tag{4.4}$$

The agreement shown in Fig. 4.4 is well within the experimental and calculation uncertainties. Note particularly that although experimental uncertainties preclude a definite determination, the data do appear to show the departure from the single Curie-Weiss-plus-temperature-independent law at high temperatures.

4.1.3 Anomolous Low Temperature Susceptibility

Vochten et al. plot the data obtained from the 15 ppm alloy as a function of 1/T to demonstrate that at temperatures below about 10 K the susceptibility deviates markedly from the high temperature Curie-Weiss-plus-temperature-independent form. It appears that at least part of the low temperature susceptibility is due to a moment with a Weiss temperature of essentially zero. The low Weiss temperature is evidenced by the temperature dependence of the susceptibility and the ease with which the moment is saturated by magnetic field.

A common source of a low temperature deviation in the form of the susceptibility is cluster effects. Similar effects seen in CuFe have been shown to be due to clusters which have a much lower Weiss temperature than isolated

impurities.[42] The direct proportionality observed between the susceptibility of the 5 ppm sample and the 15 ppm sample at all temperatures and fields appears to rule out cluster effects in this case. The anomolous temperature dependence appears to be due to the isolated impurities.

We suggest that the appearance of a moment with a Weiss temperature much lower than the high temperature value of 2.9 K may perhaps be understood in terms of the ionic model as being due to a further small splitting of the spin-orbit ground state. The sevenfold degeneracy left by the first-order spin-orbit splitting (see Fig. 4.3) may be removed by a second-order spin-orbit splitting, a spin-spin interaction, a slight departure from cubic symmetry due to a Jahn-Teller effect, or possibly a combination of these effects interacting with the applied field. At temperatures of a few degrees all of these interactions become of possible equal importance and perturbation treatments become suspect. In the following section we make some speculation on the nature of the ground state based on the impurity hyperfine data, but we do not at present know the exact nature of the low temperature structure.

The effect of a further splitting of the spin-orbit ground state, whatever its origin, is that at low temperatures the seven states left degenerate by the first-order spin-orbit coupling are not equally populated and the degrees of freedom of the impurity moment are reduced. The number of degrees of freedom appear in the exponent of the expression for the Kondo temperature, and thus even a slight reduction in the degrees of freedom lowers the Kondo temperature and hence the Weiss temperature, drastically. (For example see Ref. 32.)

4.1.4 Hyperfine Fields

If we ignore the possibility of a splitting of the spin-orbit ground

state discussed in the previous section, the $M_F = -3$ state of the $F = 3$ spin-orbit ground state is the one populated in a hyperfine field saturation measurement. We calculate the total saturation hyperfine field from Eq. 2.23. From Appendix 2 we find $(S_z')^{sat} = -2$ and $(L_z')^{sat} = -1$. $\alpha = -1$, and $k = 0.84$ from the NMR satellite fit. From Narath we have $H_L/L = 225$ kOe. H_{hf}^{sat} has been measured by Brewer[43] to be -153 kOe. From Eq. 2.23 we find $H_S/2S = +9$ kOe. Narath gives $-20 \text{ kOe} \geq (H_S/2S) \geq -130$ kOe. Clearly the agreement is poor.

We next take the approach of calculating the H_{hf}^{sat} for each of the M_F spin-orbit levels. We choose $H_S/2S = -50$ kOe because $H_S/2S$ is expected to be reasonably constant for the iron group impurities in copper,[33,44] and that is approximately the value we find for CuMn and CuFe (see Sections 4.2 and 4.3). We tabulate the results for the negative M_F states and the $M_F = 0$ state in Table 4.2; the saturation hyperfine fields for the positive M_F states are just the negatives of those given for the negative M_F states.

TABLE 4.2

Saturation Hyperfine Fields

M_F	$(S_z')^{sat}$	$(L_z')^{sat}$	H_{hf}^{sat} (kOe)
-3	-2	-1	-390
-2	-4/3	-2/3	-260
-1	-2/3	-1/3	-130
0	0	0	0

It is interesting to note that the saturation hyperfine field calculated for the $M_F = -1$ state nearly corresponds with the observed saturation hyperfine field; we might speculate that the $M_F = -1$ state is the ground

state in the high fields (up to 70 kOe) used in the saturation hyperfine field measurement. The ground state may vary with the field strength.

4.1.5 TESR Data

Before leaving the discussion of experimental evidence on CuCr we briefly comment on a TESR experiment by Monod and Schultz[41] which was interpreted as evidence that the g-factor for the Cr impurities is nearly 2. The g-factor of the F = 3, spin-orbit ground state we propose for Cr is 1.05 ±0.09. To our knowledge, this is the only experimental evidence that appears to conflict with our interpretation of CuCr.

In a TESR experiment electrons within a skin depth of one side of a thin metal sample in a static magnetic field are exposed to an alternating magnetic field at their resonant frequency to produce a transverse magnetization. The electrons diffuse through the sample, maintaining some coherence in their transverse spin components. The transverse magnetization is then detected as a signal on the other side of the sample. If there are magnetic impurities in the sample, they too will precess in the static magnetic field and those within a skin depth of the transmitter side of the sample can also be excited by the alternating field. As the conduction electrons diffuse through the sample, they may interact with the impurity moments. The total system behavior is described by two coupled equations of motion. It is the diffusing conduction electrons which are detected on the receiver side of the sample; the signal observed depends on the amount by which the impurity moments are able to influence the conduction electrons.

The phenomonological equations which Monod and Schultz used to analyze their data assume that it is necessary that the impurity moment have a g-value of nearly 2 if it is to significantly affect the observed conduction electron

resonance; the amount by which the impurity affects the conduction electron resonance is proportional to its susceptibility. By analyzing the temperature dependence of a shift they observed in the conduction electron resonance, Monod and Schultz concluded that the impurity g-value is nearly 2.

We feel that in light of the NMR satellite data we report here and the susceptibility measurement of Vochten et al.,[13] Monod and Schultz's data need to be reanalyzed. First, as discussed in Section 4.1.2, we feel that the susceptibility which Monod and Schultz used as a weighting function for the effect of the impurity atoms is in error. The Weiss temperature they used differs by a factor of three from that obtained from our satellite data and the susceptibility measurement of Vochten et al. Because the impurity susceptibility is greatest at low temperatures, the quantitative determination of the g-value is strongly influenced by the low temperature data and it is precisely at the low temperatures that the form they used for the susceptibility differs most from the form we believe to be correct. Second, Monod and Schultz did not detect the change of state which the data of Vochten et al. reveal occurs below about 10 K, and therefore took no account of it in their analysis. Again the low temperature data which is crucial in their quantitative determination of the g-value is the data for which the analysis must be considered suspect. Finally, the equations of motion which Monod and Schultz used to analyze their data took no account of the crystal field which we believe to be present at the impurity sites.

If we ignore the data Monod and Schultz obtained below 10 K because of the unknown nature of the low temperature state, the TESR data still give evidence that the resonant frequency and linewidth of the conduction electron resonance is affected by the impurity concentration although it cannot be determined whether the effects are temperature dependent. It does appear that a

fairly strong interaction exists between the conduction electrons and the impurity moments. Conventional theory[45] requires that the g-value of the impurity be nearly 2 for such a strong effect to occur; however conventional theory does not take into account crystal field effects. We suspect that the true condition for a strong interaction between the conduction electrons and impurity moments is not that they need to have the same g-value, but rather that they have energy level structures with some levels with nearly the same energy splittings in order that an energy conserving transfer of spin information (a mutual spin-flip) can occur. The ground state we propose for the Cr impurities has a g-value of about 1. The energy levels of the Cr impurities are thus spaced twice as densely as the conduction electron states; however a $\Delta M = 2$ transition on the Cr has nearly the same energy as a $\Delta M = 1$ transition for the conduction electrons. We suggest that the crystal field might provide the mechanism for allowing the $\Delta M = 2$ transition to couple to the $\Delta M = 1$ transition.

4.2 CuMn

Following Hirst we assign the $3d^5$ configuration ground state to the Mn impurity. The ground state L-S term has A_1 symmetry and thus has its orbital angular momentum quenched and is unaffected by the crystal field at the impurity site. The magnetic susceptibility is spin only and of the form of Eq. 2.8 with $S = 5/2$. Calculation of the effective moment reduction factor, η, is given in detail in Appendix 2. We find the effective moment to be 4.8 μ_B, compared with the experimental moment determined from measurements from room temperature down to a few degrees Kelvin of 4.9 $\pm$0.3 μ_B.[46] The low temperature moment measured over the temperature range of 10 mK to 0.4 K is 4.4 $\pm$0.1 μ_B which is reduced from the high temperature moment as

predicted by the renormalization group theory calculation of Krishna-murthy, Wilson and Wilkins.[3] Aton's[18] NMR satellite data show a Weiss temperature of zero--consistent within the experimental uncertainty with the value of 9.5 ±1.5 mK determined from the low temperature bulk susceptibility measurements of Hirschkoff, Symko and Wheatley.[47] Neither the NMR satellite data or the bulk measurements show any temperature independent contribution to the susceptibility.

From Eq. 2.34 with the assumption that S = 5/2 we have a saturation hyperfine field, $H_{hf}^{sat} = 5(H_S/2S)$. Davidov et al.[48] measured the value of H_{hf}^{sat} to be -280 kOe --giving $H_S/2S$ = -56 kOe. Narath[33] gives -25 kOe $\geq H_S/2S \geq$ -140 kOe. The value of $H_S/2S$ deduced for CuFe in the following section is -50 kOe.

4.3 CuFe

In this section we compare the model with data available on CuFe. By considering the alternatives, we are forced by the bulk susceptibility and NMR satellite data to conclude that Fe has the $3d^7$ configuration corresponding to that of an Fe^+ ion with the sign of the crystal field reversed from the usual assignment but consistent with that which we deduced for CuCr in Section 4.1. We find that this assignment for the ground state of Fe also produces a more satisfactory explanation of the observed hyperfine fields than the ground state usually assumed.

4.3.1 Bulk Magnetic Susceptibility and Satellite Data

We again begin by following Hirst and assign to Fe the $3d^6$ configurational ground state with T_2 symmetry (see Fig. 2.1(a)). Using the formula calculated for the susceptibility in Appendix 2, we calculate an effective

magnetic moment of 4.8 μ_B, assuming the orbital reduction factor is 1. If the orbital angular momentum is completely quenched (k = 0), the calculated effective moment is 4.1 μ_B. Steiner et al.[14] experimentally determined the value to be 3.54 ±0.08 μ_B. The error quoted reflects only data scatter and not the uncertainty in impurity concentration; however the value quoted is a composite analysis of several experiments which should help minimize the concentration error. For the calculated value of 4.1 μ_B which corresponds to k = 0 to be correct the experimental concentration must be in error by more than 30%; the value of 4.8 μ_B which corresponds to k = 1, requires that the concentration be in error by more than 80%. Especially since k is expected to be closer to 1 than 0, we conclude that the experimental concentration is probably not in error enough to make the experimentally determined moment consistent with the $3d^6$, T_2 symmetry ground state.

The T_2 ground state has a temperature independent contribution to the spin susceptibility of the form of Eq. 2.6; as a consequence the NMR satellite splittings would be expected to deviate from the low temperature Curie-Weiss law by about 30% at 300 K. Boyce and Slichter[19,20] detected no deviation from a Curie-Weiss law. The experimental uncertainties were sufficiently small that such a large deviation should have been detected.

We next try reversing the sign of the crystal field within the $3d^6$ configuration as we did for CuCr (Fig. 2.1(a) with Δ negative). The ground state then has E symmetry with the smaller temperature independent contribution to the susceptibility of the form of Eq. 2.7; however the effective magnetic moment calculated for this ground state is 4.6 μ_B, which would require a 70% error in the experimental concentration.

We conclude that the $3d^6$ assignment must be incorrect. The $3d^5$ assignment corresponds to that of CuMn which has an effective magnetic moment much

larger than CuFe. We therefore try the $3d^7$ configurational assignment.

With Hirst's assignment of the crystal field sign the $3d^7$ configurational ground state has T_1 symmetry (Fig. 2.1(b) with Δ negative) with an effective magnetic moment of about the right size, but the temperature independent contribution of the spin-orbit split ground state is again large. The NMR satellite data would be expected to show a 70% deviation from the low temperature Curie-Weiss law at 300 K which was not observed.

Finally we reverse the sign of the crystal field within the $3d^7$ configuration so that it agrees with the sign which successfully explained the CuCr data (Fig. 2.1(b)) and find we are able to obtain a reasonable fit to the CuFe data also. The ground state has A_2 symmetry. The effective magnetic moment is calculated to be 3.6 μ_B, in excellent agreement with the experimental value of 3.54 $\pm$0.08 μ_B

We assume that the orbital angular momentum and spin-orbit coupling parameter are reduced to 80% of their free ion values, similar to the reduction deduced for CuCr, and use the observed bulk susceptibility to estimate the size of the crystal field splitting. The value obtained is of the order expected. Using the estimated value of the crystal field splitting we compute the deviation from a Curie-Weiss law expected for the NMR satellite data and find it is consistent with the data.

From Appendix 2 we have that the total temperature independent contribution to the susceptibility is given by

$$\chi_{TI} = \frac{8\mu_B^2 Nk(\Delta k - \lambda)}{5\Delta^2} \quad . \tag{4.5}$$

The temperature dependent contribution is

$$X_{TD} = \frac{15\mu_B^2 N}{3}\left[\frac{1}{K_B(T+\theta)} - \frac{4k\lambda}{25\Delta^2}\right] \quad . \tag{4.6}$$

and therefore the ratio of the temperature independent contribution to the temperature dependent contribution is

$$\frac{X_{TI}}{X_{TD}} = \frac{8k(\Delta k-\lambda)K_B}{5\Delta(5\Delta-4k\lambda)}(T+\theta) \quad . \tag{4.7}$$

The observed ratio is $4.348 \times 10^{-4}(T + \theta)$.[14] The Fe^+ free ion has a spin-orbit coupling parameter of $-119\ cm^{-1}$; we assume it is reduced to $-95\ cm^{-1}$ and use $k = 0.8$. Equating Eq. 4.7 with the experimentally determined ratio, we solve for Δ and find $\Delta = 370\ cm^{-1}$; therefore the energy splitting from the A_2 ground state to the first excited crystal-field-split state is obtained from $5\Delta = 1850\ cm^{-1}$. This splitting is the equivalent of about 2700 K which is of the order of the size of crystal field expected.[25]

The temperature independent contribution to the spin susceptibility is given by

$$X_{TI}^S = -\frac{4\lambda\mu_B^2 kN}{5\Delta^2} \quad . \tag{4.8}$$

The temperature dependent spin susceptibility is just the first term of Eq. 4.6. We have, therefore:

$$\frac{X_{TI}^S}{X_{TD}^S} = -\frac{4\lambda k K_B(T+\theta)}{25\Delta^2} \quad . \tag{4.9}$$

Evaluating Eq. 4.9 with $\theta = 28$ K at $T = 300$ K, we find the ratio to be 2.0%. While the assumption that the NMR satellite data have no temperature independent contribution is certainly possible within the experimental uncertainty,

the addition of this small, temperature independent term actually improves the fit to Boyce and Slichter's data.

4.3.2 Hyperfine Field Data

Steiner et al.[14] have analyzed the Mossbauer and bulk susceptibility data and conclude $H_S/2S = -50$ kOe and $H_L/L = 470$ kOe. They analyzed the data assuming that the temperature independent contributions to the local and macroscopic susceptibility are entirely due to the orbital susceptibility and the temperature dependent contributions are due to spin only. As can be seen from the ratio of Eq. 4.8 to Eq. 4.5 with $k = 0.8$, $\lambda = -95\ cm^{-1}$ and $\Delta = 370\ cm^{-1}$, the spin susceptibility contributes about 11% of the temperature independent susceptibility, X^{TI}, and from Eq. 4.6 the orbital susceptibility contributes about 16% of the temperature dependent susceptibility, X^{TD}. Using

$$X_{mac} = -\frac{1}{H}\left[2\langle S_z\rangle + \langle L_z\rangle\right] ,$$

$$X_{loc} = -H_s\langle S_z\rangle/SH - H_L\langle L_z\rangle/LH \qquad (4.10)$$

to deduce

$$X_{loc} = X^S_{mac}\left(\frac{H_s}{2S}\right) + X^L_{mac}\left(\frac{H_L}{L}\right) , \qquad (4.11)$$

we find

$$X^{TI}_{loc} = X^{TI}_{mac}\left[0.11\left(\frac{H_s}{2S}\right) + 0.89\left(\frac{H_L}{L}\right)\right] ; \qquad (4.12)$$

$$X^{TD}_{loc} = X^{TD}_{mac}\left[1.20\left(\frac{H_s}{2S}\right) - 0.20\left(\frac{H_L}{L}\right)\right] .$$

Using the values calculated by Steiner et al. from the data for X_{loc} and X_{mac} we have $X^{TI}_{loc}/X^{TI}_{mac} = 470$ kOe and $X^{TD}_{loc}/X^{TD}_{mac} = -151$ kOe. Substituting these

values into Eq. 4.12 and solving, we find H_L/L = 533 kOe, which agrees somewhat better with Narath's[33] calculated value of 600 kOe than the value of 470 kOe given by Steiner et al., and $H_s/2S$ = -39 kOe. Narath gives $-25\ \text{kOe} \geq H_s/2S \geq -140\ \text{kOe}$.

When Hirst[44] analyzes the hyperfine fields in terms of the $3d^6$ configuration with a T_2 symmetry ground state, he finds it necessary to assume that k is less than 0.4 and the best fit value is k = 0. By his own admission such a great orbital angular momentum reduction is too much to explain as being due to the usual admixture of neighboring atomic wave functions. He postulates that a dynamic Jahn-Teller effect is present which has the effect of reducing the effective orbital angular momentum. While such an explanation is possible, we find it more satisfying to assume that the ground state has its orbital angular momentum quenched by the crystal field.

5. CONCLUSIONS

The observation of temperature independent contributions to the bulk magnetic susceptibility and NMR satellite data require the inclusion of non-degenerate orbital states in the model used for explaining the nature of the isolated Cr impurities in dilute CuCr alloys; further, the temperature independent contribution to the NMR satellite splittings, which are proportional to the spin susceptibility, requires that there be spin-orbit coupling present. The only model of 3d impurities in nonmagnetic metallic hosts which has been worked out in sufficient detail to include such fine structure is the ionic model proposed by Hirst. Our data support his model, though the details are somewhat different. Attempting to understand the experimental evidence on CuCr, CuMn and CuFe in terms of the ground state configurations proposed by Hirst, we are forced to conclude that his assignments are incorrect. By choosing the sign of the crystal field present at the impurity sites opposite of that proposed by Hirst, we find good agreement between the model and the experimental evidence when we assign the $3d^4$, $3d^5$ and $3d^7$ configurations to Cr, Mn and Fe respectively. These configurations agree with those proposed by Hirst except for Fe which he considers to be $3d^6$. Hirst[10] expects such a jump in the regular progression of $3d^n$ ground state configurations since he believes Cu to be $3d^{10}$, but he feels the jump occurs at Ni. Cohen[49] also finds this jump when he fits NMR satellite data to a potential scattering model. He finds 4.3, 5.0 and 6.9 d electrons for Cr, Mn and Fe respectively. The apparent integral jump in the number of d electrons on the impurity is additional evidence that the ground state level widths are much smaller than the virtual bound state widths calculated in a Friedel scattering model or a Hartree-Fock approximation to the Anderson model and thus

further confirms Hirst's model.

In Table 5.1 we summarize the configurations and model parameters which we have determined or estimated for the three alloys.

We would like to suggest three possible directions for future efforts to increase the understanding of these alloys: (1) further experimental study of the low temperature (less than 10 K) state of CuCr, (2) a theoretical investigation of the Kondo effect using the impurity electron-conduction electron mixing interaction suggested by Hirst (Eq. 2.3), and (3) a theoretical calculation of the spatial dependence of the NMR satellite splittings from an ionic model.

It is unfortunate that we were unable to extend our NMR satellite measurements below 8 K in view of the anomoly in the bulk susceptibility. It is possible that the very nature of the low temperature ground state prevented us from obtaining data at lower temperatures; however it might be possible to extend the measurements to lower temperatures with a pulsed NMR technique. The broad lines present at low temperatures can often be more easily observed with a pulsed method. The NMR of the Cr impurity itself should yield further information about the nature of the impurity site in the host metal if the resonance can be detected; however rapid relaxation may prevent its observation.

The nature of the Kondo effect for impurities which possess non-degenerate orbital degrees of freedom has not been investigated. It is uncertain whether the orbital degrees of freedom and spin degrees of freedom have the same Kondo temperature. It may be possible that the low temperature behavior of CuCr is due to different Kondo temperature scales for the various degrees of freedom. A renormalization group calculation would be ideal; however even a perturbation treatment should prove enlightening.

TABLE 5.1

Summary of Model Configurations and Parameters

Alloy	Config-uration	L	S	Ground state symm.	Xtal field $\Delta(cm^{-1})$	Spin-orbit $\lambda(cm^{-1})$	Orbital reduc. k	$\frac{H_s}{2S}$(kOe)	$\frac{H_L}{L}$(kOe)	μ_{eff} (μ_B)	ρJ
CuCr	$3d^4$	2	2	T_2	--	48(32)	0.84(19)	- 40[a]	225[a]	3.4(4)	- 0.11
CuMn	$3d^5$	0	5/2	A_1	--	--	--	- 56	--	4.8	- 0.33
CuFe	$3d^7$	3	3/2	A_2	370[b]	-95[c]	0.8[c]	- 39	533	3.6	- 0.31

[a] Speculation only. See Section 4.1.4.

[b] Calculated from assumed values of λ and k.

[c] Estimated at 80% of free ion values.

The ionic model appears to be quite successful in treating effects which are primarily due to intra-atomic structure such as the high temperature magnetic susceptibility; however the somewhat forbidding nature of the properly symmetrized irreducible tensor form of the impurity electron-conduction electron mixing interaction makes calculation of the spatial dependence of the conduction electron polarization difficult. McMillan[50] has suggested a compound nucleus model in which the impurity electron-conduction electron mixing interaction is treated as a scattering problem, allowing for the possibility of excited impurity states. This model holds promise of being a workable compromise. It removes the Hartree-Fock treatment of the d electrons during the time it is bound at the impurity site while retaining the H-F simplicity when it is not bound, thus removing the reasons for objection to a H-F treatment of the magnetic impurities.

APPENDIX 1: TEMPERATURE DEPENDENCE OF NMR SATELLITES

In this appendix we show that the temperature dependence of the NMR satellite splittings, ΔK, is essentially determined by the spin susceptibility of the impurity, i.e.,

$$\frac{\Delta K}{K} = g(\vec{r})X^{s}(T) \quad , \tag{A1.1}$$

where $g(\vec{r})$ is determined by the spatial dependence of the conduction electron polarization and is not a function of temperature. We consider only the part of ΔK due to the polarization of the conduction electrons through the Fermi contact interaction, which in the magnetic alloys is nearly all of ΔK for the magnetic field strengths commonly used in NMR.

We use the general form of the mixing interaction:[27]

$$H_{mix} = I \sum_{\substack{km\sigma \\ k'm'\sigma'}} a^{\dagger}_{m\sigma} a_{m'\sigma'} c^{\dagger}_{k'm'\sigma'} c_{km\sigma} \quad , \tag{A1.2}$$

where the operator $a^{\dagger}_{m\sigma}$ creates an impurity electron with z-component of angular momentum m and spin σ and the operator $c^{\dagger}_{km\sigma}$ creates a conduction electron with wave vector magnitude k, z-component of angular momentum m, and spin σ. The Fermi contact interaction between the conduction electrons and a host nucleus which is a neighbor of the impurity is given by

$$H_{en} = \frac{8\pi}{3} \gamma_e \hbar \mu_z \sum_{i=1}^{N} S_{zi} \delta(\vec{r}_i - \vec{R}) \quad , \tag{A1.3}$$

where γ_e is the electron gyromagnetic ratio, μ_z is the z-component of the nuclear magnetic moment, $\vec{R}$ is the position of the nucleus, and the sum over i is a sum over the N conduction electrons specified by positions $\vec{r}_i$. In second x quantization notation Eq. A1.3 may be written

$$H_{en} = \frac{8\pi}{3}\gamma_e\hbar\mu_z \sum_{\substack{\vec{k}\sigma \\ \vec{k}'\sigma'}} \psi^*_{\vec{k}'}(\vec{R})\psi_{\vec{k}}(\vec{R})\sigma\delta_{\sigma\sigma'}c^\dagger_{\vec{k}'\sigma'}c_{\vec{k}\sigma} \quad . \tag{A1.4}$$

(For a discussion of a similar calculation which clarifies many of the details of this calculation, see Ref. 51, p. 102 ff.) To simplify the calculation we treat the conduction electrons in a spherical approximation, i.e., we assume they are states of definite m about the impurity position. Eq. A1.4 then becomes

$$H_{en} = \frac{8\pi}{3}\gamma_e\hbar\mu_z \sum_{\substack{km\sigma \\ k'm'\sigma'}} Y^*_{2m'}(\hat{R})Y_{2m}(\hat{R})f_k(R)f_k(R)\sigma\delta_{\sigma\sigma'}c^\dagger_{k'm'\sigma'}c_{km\sigma} \quad , \tag{A1.5}$$

where we have anticipated that the impurity moment couples only to d electrons and have restricted the interaction in Eq. A1.5 to the d electrons since they alone will couple the impurity moment to the neighboring nucleus.

Let $|\alpha\rangle$ be the exact states of the impurity moment in the absence of H_{mix}; let $|\beta\rangle$ be the exact many-electron states of the conduction electrons in the absence of H_{en}. The energy of interaction between the impurity moment and the neighboring nucleus is

$$\Delta E_{\alpha\beta} = \sum_{\alpha'\beta'} \frac{\langle\alpha\beta|H_{mix}|\alpha'\beta'\rangle\langle\alpha'\beta'|H_{en}|\alpha\beta\rangle}{E_{\alpha\beta} - E_{\alpha'\beta'}} + \text{c.c.} \tag{A1.6}$$

Substituting Eqs. A1.2 and A1.5 into Eq. A1.6 and simplifying we have

$$\Delta E_{\alpha\beta} = \frac{8\pi}{3} I\gamma_e \hbar\mu_z \sum_{\substack{km\sigma \\ k'm'\beta'}} <\alpha|a^\dagger_{m\sigma}a_{m'\sigma}|\alpha><\beta|c^\dagger_{k'm'\sigma}c_{km\sigma}|\beta'>$$

$$\times <\beta'|Y^*_{2m'}(\hat{R})Y_{2m}(\hat{R})f_{k'}(R)f_k(R)\sigma c^\dagger_{km\sigma}c_{k'm'\sigma}|\beta> + c.c.$$

$$= \frac{16\pi}{3} I\gamma_e \hbar\mu_z \sum_{mm'\sigma} <\alpha|a^\dagger_{m\sigma}a_{m'\sigma}|\alpha>Y^*_{2m'}(\hat{R})Y_{2m}(\hat{R})\sigma$$

$$\times \sum_{\beta' kk'} \frac{<\beta|c^\dagger_{k'm'\sigma}c_{km\sigma}|\beta'><\beta'|c^\dagger_{km\sigma}c_{k'm'\sigma}|\beta>f_{k'}(R)f_k(R)}{E_\beta - E_{\beta'}} \quad . \qquad (A1.7)$$

$$I \sum_{mm'\sigma} \sigma a^\dagger_{m\sigma}a_{m'\sigma}Y^*_{2m'}(\hat{R})Y_{2m}(\hat{R}) \qquad (A1.8)$$

is second quantization notation for

$$I \sum_{i=1}^{n} s_{zi}\delta(\vec{r}_i - \vec{R}) \quad , \qquad (A1.9)$$

where the sum is over the n impurity d electrons with position specified by $\vec{r}_i$. (The radial dependence of the delta function is contained in the integral represented by I.) We approximate that the conduction electron states are the same as in the absence of a magnetic field; then

$$<\beta|c^\dagger_{k'm'\sigma}c_{km\sigma}|\beta'> = 0 \quad , \qquad (A1.10)$$

unless $|\beta>$ contains an electron with quantum numbers $k'm'\sigma$ and $|\beta'>$ contains an electron with quantum numbers $km\sigma$, in which case it equals 1. Let p_α be the probability that $|\alpha>$ is occupied and p_k be the probability that

the conduction electron state with wave vector magnitude k is occupied. The thermal average of Eq. A1.7 becomes:

$$\langle \Delta E_{\alpha\beta} \rangle = \frac{16\pi}{3} I\gamma_e \hbar\mu_z \sum_{\alpha} \sum_{i=1}^{n} \langle \alpha | s_{zi} \delta(\hat{r}_i' - \hat{R}) | \alpha \rangle p_\alpha$$

$$\times \sum_{kk'} \frac{p_k(1-p_{k'})f_{k'}(R)f_k(R)}{E_k - E_{k'}} \qquad \text{(A1.11)}$$

If we designate the z-component of the total spin of the impurity moment by S_z,

$$\langle S_z \rangle = \sum_{\alpha} \sum_{i=1}^{n} \langle \alpha | s_{zi} | \alpha \rangle p_\alpha \quad ; \qquad \text{(A1.12)}$$

thus Eq. A1.11 shows that the energy of interaction between the impurity moment and the neighboring nucleus is proportional to a sum like Eq. A1.12 except that it is weighted by an angular distribution function, $\delta(\hat{r}_i' - \hat{R})$.

There are three possible sources of temperature dependence in Eq. A1.11: (1) the change in population of the impurity electron states in the presence of a magnetic field which is expressed by Eq. A1.12, (2) the angular distribution function, and (3) the sum over the conduction electron states. The sum over the conduction electron states involves mainly states at the Fermi surface and thus is mainly temperature independent with a temperature dependent term of order T/T_F which can be neglected at the temperatures accessible experimentally. The angular distribution function could weight impurity states differently than the ground state and thus produce a temperature dependence; however all three satellites observed in CuCr have the same temperature dependence within the experimental uncertainties. The same is true for the satellites observed in CuMn and CuFe. We conclude that

any temperature dependence of the angular distribution is negligible. For practical purposes the temperature dependence of the interaction described by Eq. A1.11 is given solely by the temperature dependence of the impurity spin polarization; since

$$X^S = \frac{2\mu_B N}{H} < S_z > \quad , \tag{A1.13}$$

we conclude that the temperature dependence of the energy of interaction between the impurity moment and the neighboring nucleus, and hence the satellite splitting ΔK, is essentially determined by the spin susceptibility of the impurity moment.

The treatment we have given is a perturbation treatment, and thus it might be expected that it would break down near the Kondo temperature. The Kondo effect modifies Eq. A1.11 in two ways. First, the states $|\alpha>$ become significantly different from the states in the absence of the mixing; however this merely means that the spin susceptibility departs from the high temperature form. Second, the sum over the conduction electrons is changed somewhat; however since this sum is primarily temperature independent the Kondo effect has only a small effect on it. Thus Eq. A1.1 should be essentially correct for all temperatures, provided we use the spin susceptibility corrected to include the Kondo effect.

APPENDIX 2: SUSCEPTIBILITY CALCULATIONS

In this appendix we describe the calculation of the magnetic susceptibility from the ionic model for the various configurations and give the formulas for the spin susceptibility and the total susceptibility. For those configurations of particular interest for this study, we give the calculation of the reduction of the effective magnetic moment due to the impurity electron-conduction electron mixing interaction. The first two sections describe the calculations in general terms; the remaining sections give the specific cases.

A2.1 Triplet Ground State

If the crystal field ground state is a triplet, the orbital angular momentum is unquenched and the crystal field ground state degeneracy will be further split by the spin-orbit coupling. We calculate the susceptibility of the crystal field ground state only, ignoring the excited crystal field states which probably lie several thousand degrees above the ground state. Within the triplet ground state we write

$$H = H_{so} + H_z \quad , \tag{A2.1}$$

where

$$H_{so} = \alpha\lambda\vec{L}\cdot\vec{S} \quad ; \quad H_z = \mu_B H(kL_z + 2S_z) \quad , \tag{A2.2}$$

where k is an orbital reduction parameter which represents a reduction of the orbital angular momentum from that of the free ion due to the crystal environment (see Ref. 27). We have made use of the cubic cymmetry and assumed that $\vec{H}$ lies along the z-axis. Let

$$H_{so}|FM\rangle = E_F|FM\rangle \quad . \tag{A2.3}$$

To create states which are nearly eigenstates of H, we treat H_z as a perturbation on H_{so}:

$$|FM) = |FM\rangle + \sum_{F' \neq F} \frac{\langle F'M|H_z|FM\rangle}{E_F - E_{F'}} |F'M\rangle \qquad (A2.4)$$

so that

$$H|FM) \approx E_F|FM\rangle + H_z|FM\rangle \quad . \qquad (A2.5)$$

To calculate the thermal average of S_z we evaluate the trace of S_z times the density operator. As discussed in Section 2.4, since the excited crystal field states are far above the ground state, the Boltzman factor makes the contribution from these states small and we ignore their contribution, approximating the trace by a trace over the ground crystal field state only:

$$\langle S_z\rangle = \frac{1}{Z} \mathrm{Tr} S_z e^{-\beta H} \approx \frac{1}{Z} \sum_{FM} (FM|S_z e^{-\beta H}|FM)$$

$$\approx \frac{1}{Z} \sum_{FM} (FM|S_z|FM) e^{-\beta E_F}[1 - \beta\langle FM|H_z|FM\rangle]$$

$$\approx \frac{1}{Z} \sum_{FM} [(FM|S_z|FM) - \beta(FM|S_z|FM)$$

$$\times \langle FM|H_z|FM\rangle] e^{-\beta E_F}$$

$$\langle S_z\rangle \approx \left[\sum_F (2F+1) e^{-\beta E_F}\right]^{-1} \times \sum_{FM} \left[2 \sum_{F \neq F'} \frac{\langle FM|H_z|F'M'\rangle\langle F'M'|S_z|FM\rangle}{E_F - E_{F'}}\right.$$

$$\left. - \beta\langle FM|S_z|FM\rangle\langle FM|H_z|FM\rangle\right] e^{-\beta E_F} \quad . \qquad (A2.6)$$

From Eq. A2.6 we see that within the spin-orbit ground state the spin polarization has both a temperature dependent and a temperature independent term. The formula for the thermal average of L_z is obtained completely analogously to Eq. A2.6 and is identical to it with L_z substituted for S_z everywhere in the expression. The susceptibility is obtained from

$$X^S = -\frac{2\mu_B N}{H} \langle S_z \rangle \quad ; \tag{A2.7}$$

$$X^{tot} = -\frac{\mu_B N}{H} [\alpha k \langle L_z \rangle + 2\langle S_z \rangle]. \tag{A2.8}$$

We find it convenient to use a matrix transformation to obtain the matrix elements required to compute Eq. A2.6. Designate

$$M_{ij} = \langle i | H_{so} | j \rangle \qquad \text{with} \qquad |i\rangle = |LM_L SM_S\rangle \quad . \tag{A2.9}$$

We define a matrix V:

$$M' = V^{-1} M V \tag{A2.10}$$

such that M' is diagonal. Since H_{so} simply couples the fictitious angular mementum $\tilde{L}$ with the spin $\vec{S}$ to form a total fictitious momentum $\tilde{F}$, V is simply composed of Clebsch-Gordan coefficients and can be written down immediately. We define

$$Z^S_{ij} = \langle i | S_z | j \rangle \quad ; \quad Z^L_{ij} = \langle i | L_z | j \rangle \quad ; \tag{A2.11}$$

$$Z^{S'} = V^{-1} Z_S V \quad ; \quad Z^{L'} = V^{-1} Z^L V \quad .$$

The last two matrices are the matrices required for Eq. A2.6 and the analogous equation for L_z.

A2.2 Doublet or Singlet Ground State

If the crystal field ground state is a doublet or a singlet, the orbital angular momentum is quenched within the ground state. Some orbital susceptibility and some temperature independent spin susceptibility result from a mixing of the excited crystal field states into the ground state by the applied magnetic field. We treat both the spin-orbit and Zeeman interactions as perturbations on the crystal field. From group theory we know that the perturbing Hamiltonian, given by Eqs. A2.1 and A2.2 with $\alpha = 1$ since we are now using states of real angular momentum, connects an A_2 ground state only to the T_2 excited crystal field states of an F state. (Refer to Fig. 2.1.) It also connects the E ground state to the excited T_2 states of a D state. We therefore treat both cases simultaneously. We designate an unperturbed ground state by $|im_s\rangle$ (i refers to A_2 or one of the E orbital states) and calculate the corrections to the ground states to second order:

$$|im_s) = |im_s\rangle + \sum_{FM} \frac{\langle FM|H|im_s\rangle}{E_i - E_F} |FM\rangle + \sum_{\substack{FM \\ F'M'}} \frac{\langle F'M'|H|FM\rangle\langle FM|H|im_s\rangle}{(E_i - E_{F'})(E_i - E_F)} |F'M'\rangle \quad . \tag{A2.12}$$

We have written the T_2 excited states as $|FM\rangle$ because of the spin-orbit splitting within the triplet state. We calculate the thermal average of L_z, again approximating with a trace over the ground crystal field state only:

$$\langle L_z\rangle = \frac{1}{Z} \mathrm{Tr} L_z e^{-\beta H} \approx \frac{1}{Z} \sum_{im_s} [(im_s|L_z|im_s) - \beta(im_s|L_z H|im_s)] \quad . \tag{A2.13}$$

(The expansion of the exponential is legitimate since H_{so} enters only to order $\lambda/(E_i - E_F)$.) To second order in H:

$$\langle L_z \rangle = \frac{1}{Z} \sum_{im_s} \Bigg\{ \overset{(1)}{\langle im_s | L_z | im_s \rangle} + 2 \sum_{FM} \frac{\overset{(2)}{\langle im_s | L_z | FM \rangle \langle FM | H | im_s \rangle}}{E_i - E_F}$$

$$+ \sum_{\substack{FM \\ F'M'}} \frac{\overset{(3)}{\langle im_s | H | FM \rangle \langle FM | L_z | F'M' \rangle \langle F'M' | H | im_s \rangle}}{(E_i - E_F)(E_i - E_{F'})} \qquad \text{(A2.14)}$$

$$+ 2 \sum_{\substack{FM \\ F'M'}} \frac{\overset{(4)}{\langle im_s | L_z | F'M' \rangle \langle F'M' | H | FM \rangle \langle FM | H | im_s \rangle}}{(E_i - E_{F'})(E_i - E_F)}$$

$$- \beta \left[\overset{(5)}{\langle im_s | L_z H | im_s \rangle} + 2 \sum_{FM} \frac{\overset{(6)}{\langle im_s | L_z H | FM \rangle \langle FM | H | im_s \rangle}}{E_i - E_F} \right] \Bigg\} .$$

Eq. A2.14 appears rather formidable, but with an approximation and a few tricks it is easily evaluated. Since the spin-orbit splittings are much smaller than the crystal field splittings, we ignore the differences in the energies of the excited state and let $E_i - E_F = E_i - E_{F'} = \Delta$. Since the excited states are composed of orbital states which are orthogonal to the ground state, S_z does not connect the ground and excited states. Consider the terms of Eq. A2.14:

(1) = 0 since L_z vanishes in the ground state. (A2.15)

Since the sum in term (2) extends over all of the $|FM\rangle$ states, a change of basis to $|M_L M_S\rangle$ states is possible. Although the $|M_L M_S\rangle$ basis includes states in the ground state, and also states in the T_1 excited state for the crystal-field-split F states, the matrix elements of L_z between the ground state and

these states vanish. Thus

$$(2) = -\frac{2}{\Delta} \sum_{\substack{im_s \\ M_L M_S}} \langle im_s|L_z|M_L M_S\rangle\langle M_L M_S|H|im_s\rangle \quad . \tag{A2.16}$$

With the $|M_L M_S\rangle$ basis states the orbital and spin subspaces are separated and the operators L_z and S_z must appear in the trace to even powers or the trace vanishes. This allows immediate elimination of the majority of terms. Thus

$$(2) = -\frac{2\mu_B Hk}{\Delta} \sum_{iM_L} |\langle i|L_z^2|M_L\rangle|^2 \sum_{M_S} 1$$

$$(2) = -\frac{2(2S+1)\mu_B Hk\Sigma}{\Delta} \quad , \tag{A2.17}$$

where we have defined

$$\sum = \sum_{iM_L} |\langle i|L_z^2|M_L\rangle|^2 \quad . \tag{A2.18}$$

$$(3) = 0, \tag{A2.19}$$

since after a change of basis to the $|M_L M_S\rangle$ states, it is impossible to form the L_z and S_z operators both to even powers (remember S_z does not connect the ground state to the excited states).

$$(4) = \frac{4\mu_B H\lambda}{\Delta^2} \sum_{\substack{im_s \\ M_L}} \langle i|L_z|M_L\rangle\langle m_s|S_z|M_s\rangle\langle M_L|\vec{L}|i\rangle\cdot\langle m_s|\vec{S}|m_s\rangle$$

$$(4) = \frac{4\mu_B H\Sigma}{\Delta^2} \mathrm{Tr}S_z^2 \quad . \tag{A2.20}$$

$$(5) = 0 \quad . \tag{A2.21}$$

$$(6) = \frac{4\mu_B H\lambda\beta}{\Delta} \sum_{\substack{im_s \\ M_L}} \langle i|L_z|M_L\rangle\langle m_s|S_z|m_s\rangle\langle M_L|L_z|i\rangle\langle m_s|S_z|m_s\rangle$$

$$(6) = \frac{4\mu_B H\lambda\beta\Sigma}{\Delta} \mathrm{Tr}S_z^2 \quad . \tag{A2.22}$$

Collecting terms:

$$\langle L_z\rangle = -\frac{2\mu_B H\Sigma}{n_i}\left[\frac{k}{\Delta} - \frac{2S(S+1)\lambda}{3\Delta^2} - \frac{2S(S+1)\lambda\beta}{3\Delta}\right] \quad , \tag{A2.23}$$

where n_i is the orbital degeneracy of the ground state.

$$X^L = -\frac{\mu_B Nk}{H}\langle L_z\rangle \quad . \tag{A2.24}$$

$$X^L = \frac{4\mu_B^2 Nk}{n_i\Delta}\left[k - \frac{2S(S+1)\lambda}{3\Delta} - \frac{2S(S+1)\lambda}{3K_BT}\right] \quad . \tag{A2.25}$$

We obtain the spin susceptibility in the same manner. The result is

$$X^s = \frac{4\mu_B^2 NS(S+1)}{3}\left[\frac{1}{K_BT} - \frac{2k\lambda\Sigma}{n_i\Delta^2}\right] \quad . \tag{A2.26}$$

Combining the spin and orbital susceptibilities:

$$X^{tot} = 4\mu_B^2 N\left\{\frac{S(S+1)}{3K_BT}\left[1 - \frac{2\lambda k\Sigma}{n_i\Delta}\right] + \frac{k}{n_i\Delta}\left[k - \frac{4S(S+1)\lambda}{3\Delta}\right]\right\} \quad . \tag{A2.27}$$

In the following sections we give the susceptibilities of the specific configurations.

A2.3 $3d^4(T_2)$; $3d^6(T_2)$

This is the configuration we have assigned to Cr. It is also the configuration which Hirst assigns to Fe.

Within the triplet ground state the fictitious angular momentum couples to the S = 2 spin to give states of total fictitious angular momentum of magnitude 1, 2 and 3 ($\alpha = 1$). For Cr the F = 3 state lies lowest because the spin-orbit coupling is positive; for Fe the F = 1 state is lowest due to the negative spin-orbit coupling. One formula suffices for the susceptibilities of both. We give the susceptibilities in the form most convenient for computing the susceptibilities of Cr. For actual computation of the Fe susceptibilities, it is convenient (and in fact necessary for most computing devices) to multiply the numerator and denominator of the expressions given by $\exp(5\lambda\beta)$.

For the spin susceptibility we find:

$$\chi^s = [7 + 5e^{-3\lambda\beta} + 3e^{-5\lambda\beta}] \times \mu_B^2 N$$
$$\times \left\{ \frac{56}{27} \left[\frac{6(4-k)}{K_B T} + \frac{2+k}{\lambda} \right] \right.$$
$$+ e^{-3\lambda\beta} \left[\frac{25}{27} \right] \left[\frac{3(10-k)}{K_B T} + \frac{2+k}{\lambda} \right]$$
$$\left. + e^{-5\lambda\beta} [3] \left[\frac{6+k}{K_B T} - \frac{2+k}{\lambda} \right] \right\} . \qquad \text{(A2.28)}$$

The total susceptibility is given by:

$$X^{tot} = [7 + 5e^{-3\lambda\beta} + 3e^{-5\lambda\beta}] \times \mu_B^2 N$$

$$\times \left\{ \frac{28}{27} \left[\frac{3(4-k)^2}{K_B T} + \frac{(2+k)^2}{\lambda} \right] \right.$$

$$+ e^{-3\lambda\beta} \left[\frac{5}{54} \right] \left[\frac{3(10-k)^2}{K_B T} + \frac{5(2+k)^2}{\lambda} \right]$$

$$\left. + e^{-5\lambda\beta} \left[\frac{1}{2} \right] \left[\frac{(6+k)^2}{K_B T} - \frac{3(2+k)^2}{\lambda} \right] \right\} \quad . \qquad \text{(A2.29)}$$

From the expression for the total susceptibility we derive the low temperature effective magnetic moment.

For Cr the low temperature moment is:

$$\mu_{eff}^2 = \frac{4}{3} (4-k)^2 \mu_B^2 \quad . \qquad \text{(A2.30)}$$

From the fit to the NMR satellite data we have $k = 0.84 \pm 0.19$. Hence $\mu_{eff} = 3.6 \pm 0.3\ \mu_B$. We calculate the moment reduction with Eqs. 2.18 and 2.20. Using the fit from the satellite data, the Curie-Weiss temperature is 2.9 ±1.0 K; hence the Kondo temperature as defined by Eq. 2.18 is 1.45 ±0.5 K. From Eq. 2.18 we find $\rho|j| = 0.102$. Using Table 1 of Ref. 32 we insert into Eq. 2.20:

$$\rho|J| = 5(0.102) \times \frac{4.2}{17.3} \times \frac{6.63}{3.54} \times \frac{7}{15} = 0.108 \quad . \qquad \text{(A2.31)}$$

Then

$$\eta^2 = 1 + \rho J = 0.892 \qquad \text{(A2.32)}$$

and

$$\mu_{exp} = \eta\mu_{eff} = (0.892)^{1/2}(3.6) = 3.4\ \mu_B. \qquad (A2.33)$$

We increase the uncertainty since the moment reduction is only an estimate and conclude $\mu_{exp} = 3.4 \pm 0.4\ \mu_B$.

For Fe we have:

$$\mu_{eff}^2 = \frac{1}{2}(6+k)^2\mu_B^2 \qquad (A2.34)$$

μ_{eff} ranges from 4.2 to 4.9 μ_B depending on the value of k. The moment reduction calculation proceeds the same as that for Cr. $\rho|j| = 0.131$ (the Kondo temperature is 14 K) and $\rho|j| = 0.060$. $\eta^2 = 0.92$; μ_{exp} should range from 4.1 to 4.8 μ_B depending on the value of k.

A2.4 $\underline{3d^4(E);\ 3d^6(E)}$

This is the configuration Hirst assigns to Cr.

We have the susceptibilities directly from Eqs. A2.26 and A2.27. From Fig. 2.1(a) we see that the splitting between the E and T_2 states is just Δ. $\sum$ is evaluated from Eq. A2.18 and found to be equal to 2. $n_i = 2$ since the E state is a doublet. S = 2. The susceptibilities are thus given by:

$$\chi^s = 8\mu_B^2 N\left[\frac{1}{K_B T} - \frac{2k\lambda}{\Delta^2}\right]; \qquad (A2.35)$$

$$\chi^{tot} = 4\mu^2{}_B N \left\{\frac{6}{3K_B T}\left[1 - \frac{2k\lambda}{\Delta}\right] + \frac{k}{\Delta}\left[k - \frac{8\lambda}{\Delta}\right]\right\}. \qquad (A2.36)$$

We are able to conclude that this configuration does not describe Cr because the spin susceptibility has a negative temperature independent contribution, contrary to the evidence from the NMR satellite data.

To test this configuration as a possible assignment for Fe, we calculate the effective magnetic moment. From Eq. A2.36

$$\mu_{eff}^2 = 24\left(1 - \frac{2k\lambda}{\Delta}\right)\mu_B^2 \quad . \tag{A2.37}$$

From Eq. 2.18 with T_K = 14 K we obtain $\rho|j|$ = 0.1307. Using Eq. 2.19 we find $\rho|J|$ = 0.219; thus η^2 = 0.782. The second term of Eq. A2.37 comes from the orbital susceptibility (see Eq. A2.25) and thus is not reduced by the impurity electron-conduction electron mixing interaction (Eq. 2.15). Thus

$$\mu_{exp}^2 = 24\left(\eta^2 - \frac{2k\lambda}{\Delta}\right)\mu_B^2 \quad . \tag{A2.38}$$

To estimate the size of the second term we choose k = 0.8 and λ = -95 cm^{-1} (80% of the free ion value) because the orbital momentum and spin-orbit coupling were both found to be reduced about this much in Cr. For the crystal field splitting, Δ, we chose 1850 cm^{-1}, the value we deduce for Fe from the $3d^7(A_2)$ configuration. (Note that the Δ used in Eq. A2.36 is the crystal field splitting and is 5 times the Δ given in Fig. 2.1(b).) We find $\mu_{exp} = 4.6\ \mu_B$.

A2.5 $\underline{3d^5(A_1)}$

This is the configuration assigned to Mn.

The totally symmetric ground state has the orbital angular momentum quenched. The crystal field does not split the L-S ground state; the first excited state lies higher in energy by the L-S splitting, which is expected

to be on the order of 10,000 K. We ignore mixing to the excited L-S states. The susceptibility is thus spin susceptibility only; since S = 5/2

$$X^S = X^{tot} = \frac{35\mu_B^2 N}{3K_B T} \quad . \tag{A2.39}$$

To calculate the moment reduction we use T_K = 5 mK and obtain from Eq. 2.18 $\rho|j| = 0.0656$. Because the L-S ground state is not split by the crystal field, $\rho|J| = 5 \times \rho|j| = 0.328$. $\eta^2 = 0.672$; $\mu_{exp} = 4.8\ \mu_B$.

A2.6 $3d^7(A_2);\ 3d^3(A_2)$

This is the configuration we assign to Fe.

The susceptibilities come directly from Eqs. A2.26 and A2.27. From Fig. 2.1(b) we see that the crystal field splitting is 5Δ; we replace the Δ in Eq. A2.26 and A2.27 with 5Δ to express the susceptibilities in terms of the crystal field parameter. From Eq. A2.18 we find $\sum = 2$. $n_i = 1$ because the ground state is a singlet. S = 3/2. Therefore:

$$X^S = 5\mu_B^2 N \left[\frac{1}{K_B T} - \frac{4k\lambda}{25\Delta^2}\right] \quad ; \tag{A2.40}$$

$$X^{tot} = 4\mu_B^2 N \left\{\frac{(15/4)}{3K_B T}\left[1 - \frac{4k\lambda}{5\Delta}\right] + \frac{2k}{5\Delta}\left[k - \frac{\lambda}{\Delta}\right]\right\} \quad . \tag{A2.41}$$

From Eq. A2.41 we have:

$$\mu_{eff}^2 = 15\left(1 - \frac{4k\lambda}{5\Delta}\right)\mu_B^2 \quad . \tag{A2.42}$$

From Eq. 2.18 with T_K = 14 K we obtain $\rho|j| = 0.1307$. Using Eq. 2.19 we find $\rho|J| = 0.309$; thus $\eta^2 = 0.691$. The second term of Eq. A2.37 comes

from the orbital susceptibility (see Eq. A2.25) and thus is not reduced by the impurity electron-conduction electron mixing interaction (Eq. 2.15). Thus

$$\mu_{exp}^2 = 15\left(\eta^2 - \frac{4k\lambda}{5\Delta}\right)\mu_B^2 \quad . \tag{A2.43}$$

To estimate the size of the second term we choose k = 0.8 and $\lambda = -95\ cm^{-1}$ as explained in Section A2.4. In Section 4.3.1 we estimated $\Delta = 370\ cm^{-1}$. We obtain $\mu_{exp} = 3.6\ \mu_B$.

A2.7 $3d^7(T_1)$; $3d^3\ (T_1)$

Within the triplet ground state the fictitious angular momentum couples to the S = 3/2 spin to give states of total fictitious angular momentum of magnitude 1/2, 3/2 and 5/2 ($\alpha = -3/2$). If this configuration were the configuration of Fe, the F = 1/2 state would lie lowest because the spin-orbit coupling is negative. We find for the susceptibilities:

$$\chi^s = [1 + 2e^{9\lambda\beta/4} + 3e^{6\lambda\beta}]^{-1} \times \mu_B^2 N$$

$$\times \left\{ \frac{5}{162}\left[\frac{9(10+3k)}{K_B T} - \frac{16(4+3k)}{\lambda}\right] \right. \tag{A2.44}$$

$$+ e^{9\lambda\beta/4}\left[\frac{22}{2025}\right]\left[\frac{45(11-3k)}{K_B T} + \frac{16(4+3k)}{\lambda}\right]$$

$$\left. + e^{6\lambda}\left[\frac{1}{50}\right]\left[\frac{315(2-k)}{K_B T} + \frac{16(4+3k)}{\lambda}\right]\right\} \quad ;$$

$$\chi^{tot} = [1 + 2e^{9\lambda\beta/4} + 3e^{6\lambda\beta}]^{-1} \times \mu_B^2 N$$

$$\times \left\{ \frac{1}{324} \left[\frac{9(10+3k)^2}{K_B T} - \frac{40(4+3k)^2}{\lambda} \right] \right. \tag{A2.45}$$

$$+ e^{9\lambda\beta/4} \left[\frac{2}{2025} \right] \left[\frac{45(11-3k)^2}{K_B T} + \frac{44(4+3k)^2}{\lambda} \right]$$

$$\left. + e^{6\lambda\beta} \left[\frac{1}{100} \right] \left[\frac{315(2-k)^2}{K_B T} + \frac{8(4+3k)^2}{\lambda} \right] \right\} .$$

From Eq. A2.45 we have:

$$\mu_{eff}^2 = \frac{(10+3k)^2}{12} \mu_B^2 . \tag{A2.46}$$

Hirst has not calculated the Born approximations to the resistivity necessary for Eq. 2.20; we do not calculate the moment reduction. μ_{eff} ranges from 2.9 to 3.8 μ_B depending on the value of k. The effective moment is thus consistent with the Fe experimental moment; however as pointed out in Section 4.3.1 the spin susceptibility has a temperature independent contribution which is much too large to be consistent with the NMR satellite data.

APPENDIX 3: MODULATION CONTROLLER

The practical limitation on sensitivity in broad line NMR is frequently spurious effects on the baseline rather than the masking of the signal by thermal noise. In this appendix we describe a simple circuit we have used to reduce spurious baseline effects by a factor of three hundred. Specifically, this circuit reduces baseline effects which result when the amplitude of the modulating magnetic field is not constant throughout the field sweep.

The modulation coils on the low-field, iron core magnet spectrometer are wound directly on the pole faces of the magnet. If the modulation coils are merely driven with constant power, as the magnetic field is swept the saturation of the iron core of the magnet changes and therefore the modulation amplitude changes. When the magnetic field is swept several hundred oersted in order to observe a broad NMR line, especially near the high field end of the magnet where most NMR experiments are done, the saturation of the iron core changes significantly and the modulation amplitude varies about 3% per 100 Oe. swept.

Despite careful experimental design, there is usually a spurious signal whose amplitude is proportional to the modulation amplitude, present at the input to the lock-in amplifier. The most common source of such a signal is vibrations caused by the modulation field which modulate the impedance of the bridge arm at the driving modulation frequency and hence produce a spurious signal. If the modulation amplitude is constant, the constant spurious signal can be offset at the lock-in (providing it is not too large), and the baseline remains nearly flat; however if the modulation amplitude changes, the amplitude of the spurious signal tracks the changing

modulation amplitude and a changing baseline results. Since the saturation of the iron core is by no means linear with the magnetic field strength, the modulation amplitude changes non-linearly as the field is swept and a curving baseline results. The curvature of the baseline can be sufficient that it limits the detection of the NMR signal before the limits of the thermal noise are reached.

The feedback circuit we used reduces the modulation amplitude variation to less than 0.1%; it thus reduces the change in the modulation amplitude by a factor of 300 over a field sweep of 1 kOe. With the modulation amplitude controlled to this precision other experimental effects become the limiting factors in the baseline curvature.

An added benefit of the control circuit is that it significantly reduces baseline drift, i.e., slow changes in the lock-in offset voltage caused by gradual changes in the modulation amplitude produced by such effects as thermal drifts in the audio power amplifiers.

Figure A3.1 is a schematic of the circuit. The CA3028 integrated circuit is used as an automatic gain control inserted between the lock-in reference voltage output and the input to the power amplifiers. The gain is adjusted by the feedback loop consisting of a pickup coil (with a nonmagnetic core to avoid introduction of a field distortion) and an operational amplifier comparator to maintain the modulation amplitude constant. The modulation amplitude is adjusted by changing the bias on the non-inverting input to the operational amplifier.

The gain of the integrated circuit is a very nonlinear function of the voltage applied to pin 7. We have found 2 to 6 V. to be a usable operating range. When setting the desired modulation, the modulation amplitude

adjustment is first set to zero and the lock-in reference voltage is set higher than is expected to be necessary. The modulation amplitude desired is selected by increasing the modulation amplitude adjustment while monitoring the test point with the switch in the "mod" position. The test point is then switched to the "gain" position and the lock-in reference voltage is reduced until the gain voltage just reaches 6 V. at its maximum during a field sweep. At the highest modulation amplitudes we have used (50 Oe. p-p) in large field sweeps (1 kOe.) we have found it necessary to increase the lock-in reference voltage to the point that the output of the IC is completely clipped and furnishes the power amplifier with a square wave; however since the modulation coils are tuned to the desired modulation frequency in order to deliver maximum modulation power, the field modulation has less than 1% second harmonic and less than 4% third harmonic distortion. Because lock-in detection at the modulation frequency is used, the distortion results in no perceptible distortion of the signal or increase in the noise.

Figure A3.1: Schematic of the modulation amplitude controller.

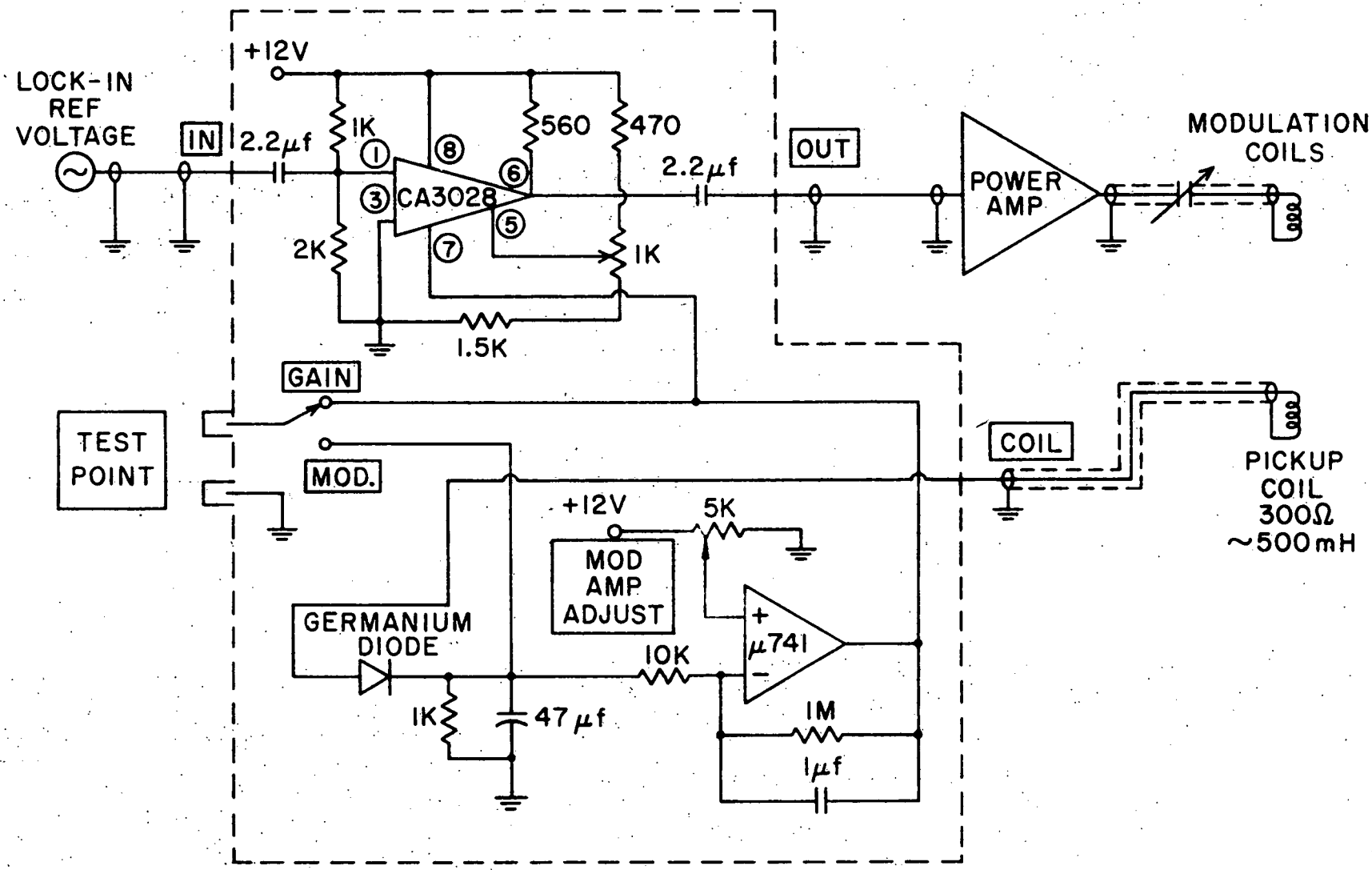
+12V
LOCK-IN
REF
VOLTAGE
IN
2.2μf
1K
560
470
2.2μf
OUT
POWER
AMP
MODULATION
COILS
CA3028
2K
1K
1.5K
GAIN
TEST
POINT
MOD.
COIL
PICKUP
COIL
300Ω
~500mH
+12V
5K
MOD
AMP
ADJUST
GERMANIUM
DIODE
10K
μ741
1K
47μf
1M
1μf

APPENDIX 4: EFFECT OF LOCK-IN TIME CONSTANT ON OBSERVED SIGNAL

In this appendix we discuss the effect which a low-pass filter has on a signal. We give the results of a numerical computation of the effect of the -12 db/octave filter of a lock-in amplifier on the derivatives of Gaussian and Lorentzian line shapes, two line shapes commonly encountered in magnetic resonance experiments. We show the relative signal-to-noise ratios and distortion of each line shape as a function of the filter time constant. We empirically observe that a universal function can be used to compute the amount by which the filter shifts the zero crossing of both line shapes, and hence have a technique for determining the true resonant field from the observed signal.

A simple RC low-pass filter is a -6 db/octave filter whose effect on a signal can be described by:

$$V_o(t) = \int_{-\infty}^{\infty} dt' g(t,t') V_i(t') \quad , \tag{A4.1}$$

where $V_i(t)$ is the signal at the input of the filter, $V_o(t)$ is the signal at the output of the filter, and the Green's function is given by:

$$g(t,t') = \begin{cases} 0 & \text{for } t < t' \quad . \\ \frac{1}{RC} e^{-(t-t')/RC} & \text{for } t \geq t' \quad . \end{cases} \tag{A4.2}$$

The -12 db/octave filter in a lock-in amplifier consists of two RC low-pass filters in series; however the first filter is in the feedback circuit of an operational amplifier to prevent the second filter from loading the first. The effect of this type of -12 db/octave filter on a signal is described by:

$$V_o(t) = \int_{-\infty}^{\infty} dt' g(t,t') \int_{-\infty}^{\infty} dt'' g(t',t'') V_i(t'') \quad . \tag{A4.3}$$

Upon substitution of Eq. A4.2 into Eq. A4.3 and integration by parts we obtain:

$$V_o(t) = \frac{1}{(RC)^2} \int_{-\infty}^{t} dt' V_i(t')(t-t')e^{-(t-t')/RC} \quad . \tag{A4.4}$$

This equation forms the basis for the rest of the analysis discussed in this appendix.

Two line shapes frequently encountered in magnetic resonance experiments are the Lorentzian and the Gaussian. With small amplitude modulation and lock-in detection, the signal observed is nearly proportional to the derivative of the unmodulated signal. We limit this analysis to the derivatives of the Lorentzian and Gaussian absorption line shape:

Gaussian: $$V_i(t) = -\frac{t}{\sqrt{2\pi}} e^{-t^2/2} \quad ; \tag{A4.5}$$

Lorentzian: $$V_i(t) = \frac{-2\sqrt{3}t}{\pi(t^2+3)^2} \quad . \tag{A4.6}$$

Using these two functions as input signals we have computed the output signals from Eq. A4.4 numerically, and analyzed how the output varies as a function of RC.

Three factors are of primary interest to us for application to experiment: (1) the signal-to-noise ratio, (2) the amount of line shape distortion, and (3) the shift in the apparent resonant position. We define the signal as the peak-to-peak amplitude of $V_o(t)$. We define the resonant position by the zero-crossing of $V_o(t)$. The quantification of line shape distortion is somewhat more arbitrary than the first two definitions; we

have chosen to define:

$$\text{Distortion} = 1 - \frac{|V_o|_{min}}{(V_o)_{max}} \quad . \qquad \text{(A4.7)}$$

In Fig. A4.1 we have plotted the signal-to-noise ratio and distortion for both line shapes. Note that the maximum signal-to-noise ratio is obtained when the time constant is adjusted such that 3 to 4 time constants are spent sweeping through the linewidth (we define the linewidth to be the width between the peaks of the derivative); however when the signal-to-noise ratio is maximized the signal shape suffers about 15% distortion. If distortion is to be held below 5%, approximately 7 time constants per linewidth are required; a 1% distortion tolerance requires about 14 time constants per linewidth. Since the amount of averaging time required is inversely proportional to the square of the signal-to-noise ratio, the loss of signal-to-noise required to keep signal distortion to a minimum can result in a significant increase in the required averaging time. One way to keep distortion to a minimum and compensate for the reduced signal-to-noise ratio is to use a larger modulation amplitude and use a technique such as that described in Ref. 39 to correct for the distortion produced by a large modulation amplitude.

When analyzing experimental data the most readily available measure of the resonance linewidth is not the true linewidth but rather the linewidth of the observed signal; therefore to facilitate data analysis we have calculated the amount by which the zero-crossing of the resonance is shifted by the filter in terms of a fraction of the observed linewidth. The results for the Gaussian line shape are given in Table A4.1; the results for the Lorentzian line shape are given in Table A4.2. In Fig. A4.2 we have plotted both sets of

Figure A4.1: The signal-to-noise ratio and distortion are plotted versus the number of time constants per linewidth for the Lorentzian (solid curves) and Gaussian (dashed curves) line shapes. The signal-to-noise ratio is in arbitrary units.

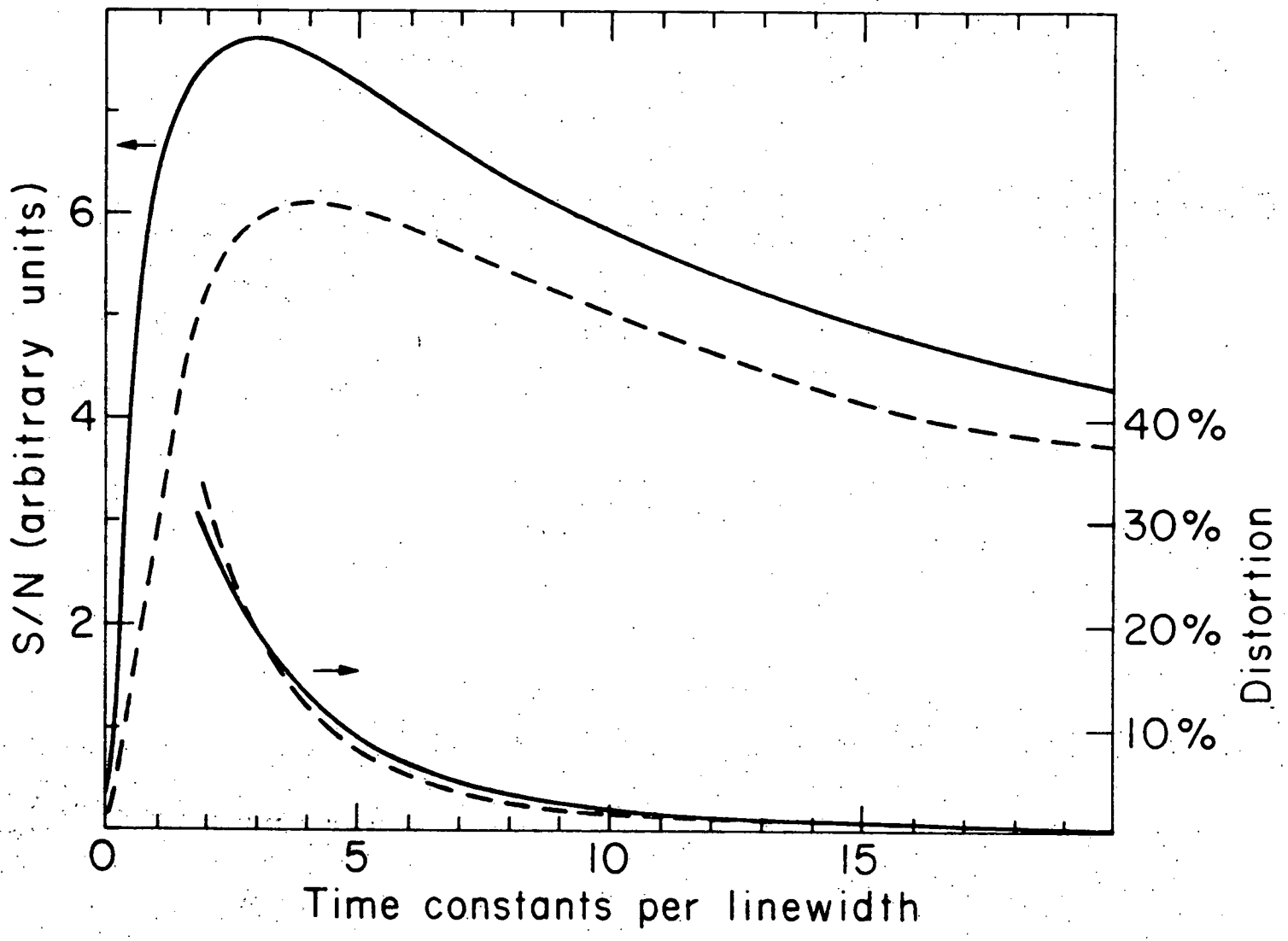
S/N (arbitrary units)
6
4
2
0
5
10
15
Time constants per linewidth
40%
30%
20%
10%
Distortion

TABLE A4.1

Zero-crossing Shift of Gaussian Line Shape

The zero-crossing shift produced by the lock-in -12 db/ octave filter is given in terms of a fraction of the observed linewidth for a Gaussian line shape.

time constants / obs. width	zero shift / obs. width
2.768	0.5350
3.672	0.4465
4.604	0.3775
5.545	0.3251
6.495	0.2845
7.455	0.2521
8.416	0.2220
10.355	0.1864
20.220	0.0979

TABLE A4.2

Zero-crossing Shift of Lorentzian Line Shape

The zero-crossing shift produced by the lock-in -12 db/ octave filter is given in terms of a fraction of the observed linewidth for a Lorentzian line shape.

time constants / obs. width	zero shift / obs. width
3.351	0.4637
4.212	0.3967
5.098	0.3433
6.000	0.3004
6.924	0.2660
7.850	0.2381
10.685	0.1800
20.430	0.0969

Figure A4.2: The data given in Tables A4.1 and A4.2 are plotted on the same curve (solid curve). The dashed curve represents a zero-crossing shift of two time constants.

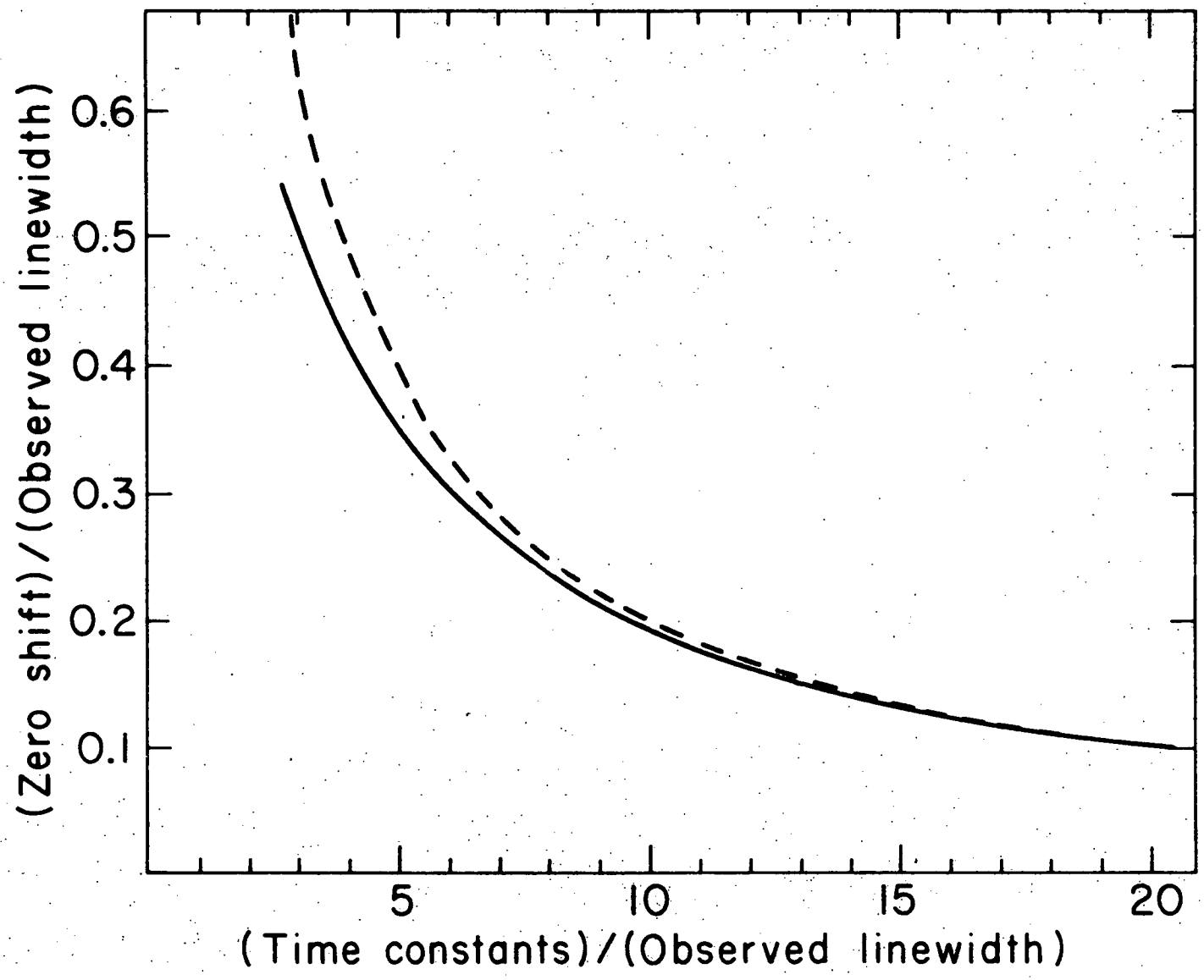
(Zero shift)/(Observed linewidth)
0.6
0.5
0.4
0.3
0.2
0.1
5
10
15
20
(Time constants)/(Observed linewidth)

calculations on the same graph; we find empirically that both sets of data fall on the same smooth curve. Also plotted in the same figure is the curve which represents a zero-crossing shift of two time constants. Note that for a large number of time constants in the linewidth the zero-crossing is just shifted two time constants; for fewer time constants per linewidth the zero-crossing is shifted less than two time constants.

We have not determined the cause of the fact that the zero-shift for both line shapes can be described by the same function when expressed in terms of the observed linewidth. The same relationship does not obtain if the zero-crossing shift is expressed in terms of the true linewidth. The fact that the Lorentzian line shape is broadened more than 20% more than the Gaussian line shape for the longest time constants used leads us to believe that the zero-crossing shift must scale proportional to the line broadening for a wide variety of line shapes. We have tested the function plotted in Fig. A4.2 against the Cu^{63} resonance in dilute alloys of iron group impurties in Cu. The line shapes in these alloys vary with concentration and type of impurity; they are neither Lorentzian or Gaussian and in fact for the more concentrated alloys they are assymetrical. We have varied the time constant by over two orders of magnitude. The observed resonance shifts all agreed with the plotted function to within the experimental resolution.

We have used the function plotted in Fig. A4.2 to correct the observed zero-crossings in our NMR satellite data. Because we were interested only in the resonant position of the satellite resonances and not their detailed line shape, we were able to use about 4 time constants per linewidth in order to maximize the signal-to-noise ratio and obtain the true zero-crossing from Fig. A4.2.

REFERENCES

1. C. Zener, Phys. Rev. 81, 440 (1951).
2. J. Kondo, Progr. Theor. Phys. (Kyoto) 32, 37 (1964).
3. H. R. Krishna-murthy, K. G. Wilson, and J. W. Wilkins, Phys. Rev. Lett. 35, 1101 (1975).
4. J. Friedel, Phil. Mag. 43, 153 (1952).
5. P. W. Anderson, Phys. Rev. 124, 41 (1961).
6. A. Blandin, J. Appl. Phys. 39, 1285 (1968).
7. B. Coqblin and A. Blandin, Adv. Phys. 17, 281 (1968).
8. J. R. Schrieffer and P. A. Wolff, Phys. Rev. 149, 491 (1966).
9. L. L. Hirst, Z. Physik 241, 9 (1971).
10. L. L. Hirst, AIP Conf. Proc. No. 24, 11 (1975).
11. A. J. Heeger, Solid State Physics, Vol. 23, Eds. F. Seitz, D. Turnbull, and H. Ehrenreich (Academic Press, New York and London, 1969).
12. H. G. Hoeve and D. O. Van Ostenburg, Phys. Rev. Lett. 26, 1020 (1971).
13. M. Vochten, M. Labro, and S. Vynckier, Physica 86-88B, 467 (1977).
14. P. Steiner, S. Hufner, and W. V. Zdrojewski, Phys. Rev. B10, 4704 (1974).
15. D. C. Abbas, D. M. Follstaedt, T. S. Stakelon, and C. P. Slichter, unpublished data on CuSc, 1974.
16. D. M. Follstaedt, D. C. Abbas, T. S. Stakelon, and C. P. Slichter, Phys. Rev. B14, 47 (1976).
17. D. M. Follstaedt and C. P. Slichter, to be published in Phys. Rev., 1977.
18. T. J. Aton, Ph.D. Thesis, University of Illinois, 1976 (unpublished).
19. J. B. Boyce and C. P. Slichter, Phys. Rev. Lett. 32, 61 (1974).
20. J. B. Boyce and C. P. Slichter, Phys. Rev. B13, 379 (1976).
21. T. S. Stakelon and C. P. Slichter, Phys. Rev. B14, 3793 (1976).
22. D. V. Lang, J. B. Boyce, D. C. Lo, and C. P. Slichter, Phys. Rev. Lett. 29, 776 (1972).

23. D. V. Lang, D. C. Lo, J. B. Boyce, and C. P. Slichter, Phys. Rev. B9, 3077 (1974).

24. D. C. Lo, D. V. Lang, J. B. Boyce, and C. P. Slichter, Phys. Rev. B8, 973 (1973).

25. L. L. Hirst, Archives des Sciences 27, 279 (1974).

26. Y. Yafet, Phys. Lett. 26A, 481 (1968).

27. A. Abragam and B. Bleaney, Electron Paramagnetic Resonance of Transition Ions (Clarendon Press, Oxford, 1970).

28. L. L. Hirst, Z. Physik 244, 230 (1971).

29. L. L. Hirst, Adv. in Phys. 21, 759 (1972).

30. J. Kondo, Solid State Physics, Vol. 23, Eds. F. Seitz, D. Turnbull, and H. Ehrenreich (Academic Press, New York and London, 1969).

31. K. Wilson, Rev. Mod. Phys. 47, 773 (1975).

32. L. L. Hirst, Int. J. Magn. 2, 213 (1972).

33. A. Narath, CRC Critical Rev. in Sol. St. Sci. 3, 1 (1972).

34. J. B. Boyce, Ph.D. Thesis, University of Illinois, 1972 (unpublished).

35. D. M. Follstaedt, Ph.D. Thesis, University of Illinois, 1975 (unpublished).

36. L. J. Neuringer and L. G. Rubin in Temperature, vol. 4, pt. 2, 1085 (Instrument Society of America, Pittsburgh, 1972).

37. J. M. Swartz and J. R. Gaines in Temperature, vol. 4, pt. 2, 1117 (Instrument Society of America, Pittsburgh, 1972); R. Berman in Temperature, vol. 4, pt. 3, 1537 (Instrument Society of America, Pittsburgh, 1972); L. L. Sparks and R. L. Powell, J. of Research of NBS 76A, 263 (1972).

38. H. A. Buckmaster and J. C. Dering, J. Appl. Phys. 39, 4486 (1968); H. A. Buckmaster and J. D. Skirrow, J. Mag. Res. 5, 285 (1971); H. A. Buckmaster and J. D. Skirrow, J. Appl. Phys. 42, 1225 (1971); R. J. Hanisch and G. P. Hughes, Rev. Sci. Instrum. 46, 1262 (1975).

39. R. A. Wind and S. Emid, J. Phys. E: Sci. Instrum. 8, 281 (1975).

40. H. G. Hoeve and D. O. Van Ostenburg, Phys. Rev. Lett. 26, 1020 (1971).

41. P. Monod and S. Schultz, Phys. Rev. 173, 645 (1968).

42. J. L. Tholence and R. Tournier, Phys. Rev. Lett. 25, 867 (1970).

43. W. D. Brewer, Phys. Lett. 49A, 397 (1974).

44. L. L. Hirst, Z. Physik 245, 378 (1971).

45. S. E. Barnes, J. Phys. F: Metal Phys. 6, 1713 (1976); J. H. Pifer and R. T. Longo, Phys. Rev. B4, 3797 (1971).

46. C. M. Hurd, J. Phys. Chem. Solids 30, 539 (1968).

47. E. C. Hirschkoff, O. G. Symko, and J. C. Wheatley, J. Low Temp. Phys. 5, 155 (1971).

48. D. Davidov, C. Rettori, R. Orbach, A. Dixon, and E. P. Chock, Phys. Rev. B11, 3546 (1975).

49. J. D. Cohen, submitted to Phys. Rev. Lett., 1977.

50. W. McMillan, private communication, 1977.

51. C. P. Slichter, Principles of Magnetic Resonance (Harper and Row, New York, Evanston, and London, 1963).

VITA

Daniel Cornelius Abbas was born [redacted], [redacted]. He graduated as valedictorian of Forreston Community High School, Forreston, Illinois in May 1965. He entered Calvin College in Grand Rapids, Michigan, with a Calvin College Freshman Honor Scholarship. While at Calvin he was awarded a Calvin Alumni Scholarship, a Calvin Upperclassman Scholarship, and a Dow Chemical Scholarship. He received a Bachelor of Arts degree in May 1969 with a double major--physics and mathematics.

He received a teaching assistantship at the University of Illinois and was awarded a Master of Science degree in August 1970.

He was drafted into the U. S. Army and spent eighteen months as a Physical Science Assistant. After being released from active duty in May 1972, he held the position of Research Physicist at the U. S. Army Tank-Automotive Command in Warren, Michigan.

He returned to the University of Illinois in January 1974 where he has been a research assistant.

In June 1977 he will assume a position as Senior Research Physicist with Eastman Kodak Company, Rochester, New York.